Applied Physics Reviews

REVIEW ARTICLE | OCTOBER 30 2026

Coupling single spins to superconducting circuits

Special Collection: Quantum Sensing

M. Stern ✉ ; X. Xue ; E. Flurin ; C. K. Andersen ; L. M. K. Vandersypen ; P. Bertet

Check for updates

Appl. Phys. Rev. 13, 041316 (2026)
https://doi.org/10.1063/5.0342292

View Online
Export Citation

Articles You May Be Interested In

Microwave transmission and dynamical response of three on-chip superconducting resonators coupled to the same molecular spin ensemble

Low Temp. Phys. (July 2026)

Operating a bistable qubit

Appl. Phys. Rev. (October 2026)

31 October 2026 16:32:36

AIP Publishing

Special Topics Open for Submissions

Learn More

AIP Publishing

Applied Physics Reviews REVIEW pubs.aip.org/aip/are

Coupling single spins to superconducting circuits

Cite as: Appl. Phys. Rev. **13**, 041316 (2026); doi: 10.1063/5.0342292
Submitted: 6 May 2026 · Accepted: 14 October 2026 ·
Published Online: 30 October 2026

View Online Export Citation CrossMark

M. Stern,[1,a)] X. Xue,[2] E. Flurin,[3] C. K. Andersen,[2] L. M. K. Vandersypen,[2] and P. Bertet[3]

AFFILIATIONS

[1]Department of Physics, Technion-Israel Institute of Technology, Haifa 32000, Israel
[2]QuTech and Kavli Institute of Nanoscience, Delft University of Technology, Delft, The Netherlands
[3]Quantronics Group, SPEC, IRAMIS, DSM, CEA Saclay, Gif-sur-Yvette, France

Note: This paper is part of the APR Special Topic on Quantum Sensing.
[a)]**Author to whom correspondence should be addressed:** m.stern@technion.ac.il

ABSTRACT

Coupling single spins to superconducting circuits represents a powerful route toward scalable hybrid quantum technologies. At the intersection of quantum information processing, nanoscale sensing, and condensed matter physics, this emerging research direction aims to unite the best qualities of two very different quantum systems. Spins—whether associated with electrons, nuclei, or defects—are among the most coherent quantum systems known, with coherence times that can exceed seconds. However, their weak interaction with electromagnetic fields makes them notoriously difficult to control and read out individually. Superconducting circuits, on the other hand, offer exceptional control, scalability, and strong coupling to electromagnetic fields, but they tend to suffer from shorter coherence times. Bridging these two platforms can yield hybrid quantum systems that harness the best of both worlds: the long-lived quantum memory of spins and the fast, flexible control of superconducting devices. An additional key motivation for integrating single spins with superconducting circuits is the ability to perform spectroscopy at the nanoscale, enabling the investigation of quantum systems with unprecedented spatial and energy resolution. Spins, due to their sensitivity to magnetic and electric fields, serve as exquisite local probes of their environment. This synergy not only offers powerful tools for probing quantum phenomena at the nanoscale but also opens the possibility of hybrid quantum processors combining long-lived spin states with fast superconducting-circuit control.

© 2026 Author(s). All article content, except where otherwise noted, is licensed under a Creative Commons Attribution (CC BY) license (https://creativecommons.org/licenses/by/4.0/). https://doi.org/10.1063/5.0342292

TABLE OF CONTENTS

I. INTRODUCTION 1
II. SPINS IN GATE-DEFINED QUANTUM DOTS 2
A. Time-domain 5
B. Longitudinal coupling 5
C. Other application: Fast readout 6
III. ANDREEV SPIN QUBITS 7
IV. SPIN-RESONATOR MAGNETIC COUPLING 9
V. FLUX QUBITS COUPLED TO IMPURITY DONORS . 11
VI. CONCLUSIONS 13

I. INTRODUCTION

Superconducting circuits and microscopic spin systems offer highly complementary resources. Superconducting devices are well coupled to microwave photons and thus provide fast control and sensitive readout.[1,2] Spins, by contrast, are localized quantum systems with potentially long coherence times and a high sensitivity to their local environments. Coupling individual spins to superconducting circuits is therefore attractive both as a route toward hybrid quantum processors, in which spins provide long-lived quantum states connected by microwave circuitry, and as a tool for nanoscale spectroscopy, where the spin itself acts as a microscopic probe.

In the early development of spin–superconducting-circuit hybrids, experiments mainly focused on large spin ensembles.[3–8] In that regime, the coupling to the microwave field is collectively enhanced by the number of spins,[9] partially compensating for the extremely weak magnetic moment of each individual spin. This collective enhancement made it possible to observe coherent coupling between spin ensembles and superconducting resonators.[3,6] However, detecting or manipulating the magnetic resonance signal of a single microscopic spin was long considered out of reach. The central challenge addressed in this review is how this limitation can be overcome, and how superconducting circuits can be engineered to interact with individual spins rather than macroscopic ensembles.

At the single-spin level, the main difficulty is that magnetic dipole interactions are typically several orders of magnitude weaker than electric-dipole interactions. This makes achieving strong or even

31 October 2026 16:32:36

© Author(s) 2026

detectable coupling to an individual spin inherently difficult. To address this issue, several coupling strategies have emerged:

1. Direct magnetic dipole coupling involves interfacing the spin's magnetic moment with the magnetic field of a specially engineered superconducting resonator or qubit. This approach is broadly applicable to a wide range of spin systems, including localized spins in defects, dopants, or molecules. However, due to the weak vacuum magnetic field fluctuations at the spin location, the resulting coupling strength is typically limited to the few Hz–100 kHz range.
2. Indirect coupling via electric-dipole transitions is a promising alternative for spin systems where spin-orbit coupling or hybridization enables an effective electric-dipole interaction. For example, conduction electron spins in quantum dots or donors in semiconductors can couple to the resonator's electric field via spin-charge hybridization. This method can yield significantly stronger couplings (up to 10's of MHz in favorable configurations), but often at the cost of reduced spin coherence due to charge noise.
3. A third, more specific mechanism appears in Andreev spin qubits, where the spin degree of freedom couples to the superconducting circuit through the phase-dependent Andreev spectrum of a weak link. Due to the spin-orbit coupling of the weak link, changing the spin state modifies the Josephson admittance, or equivalently the spin-dependent supercurrent, seen by the surrounding circuit.

In this review, we will consider different recent approaches ranging from semiconductor quantum-dot spins coupled to microwave resonators through spin-charge hybridization to Andreev qubits where the spin degree of freedom modulates the Josephson response across a weak link, from erbium ions in calcium tungstate detected by a single microwave-photon detector to bismuth donors in silicon coupled to superconducting flux qubits. We do not attempt a comprehensive review of spin ensembles, optically detected single defects without superconducting microwave circuitry, or platforms where only theoretical proposals exist; these are important but fall outside the scope of a focused comparison of experimentally demonstrated single-spin/superconducting-circuit interfaces. Throughout the review, we emphasize not only the coupling strength itself, but also the physical regime in which the coupling is used. Depending on the platform, the relevant figure of merit may be coherent exchange, cooperativity, readout fidelity, radiative branching ratio, or the degree of circuit-induced back-action on the spin. This distinction is important because superconducting circuits may act as coherent quantum buses, fast detectors, or control elements, and these different roles impose different requirements on coupling strength, linewidth, coherence, magnetic-field compatibility, and scalability.

II. SPINS IN GATE-DEFINED QUANTUM DOTS

Spin qubits encoded using electrons or holes confined in semiconductor quantum dots[10,11] exhibit good coherence properties,[12] are compatible with standard CMOS technologies, and have a small footprint, making them suitable for scaling up and integration into large-scale quantum processors.[13] These advantages have been supported by recent demonstrations of high-fidelity quantum gates[14–16] and realizations of multiple qubit arrays in one- and two-dimensions.[17–20]

Theoretical proposals for coupling semiconductor spin qubits to microwave resonators established several of the mechanisms now used in devices. Early work considered coherent coupling of localized spins through cavity modes and superconducting transmission-line resonators, showing how microwave photons could mediate long-distance spin–spin interactions.[21,22] Subsequent theory explored how the intrinsically weak magnetic-dipole interaction could be enhanced by converting spin motion into an electric dipole through spin–orbit coupling, spin–charge hybridization, or engineered magnetic-field gradients.[23–27] These works identified the central design compromise that remains important today: increasing the electric-dipole character enhances the spin–photon coupling strength, but also increases sensitivity to charge noise and cavity-induced relaxation. Other works have proposed methods for achieving strong coupling of so-called exchange-only qubits, where the qubit is operated purely through electrically tunable exchange interactions. This theoretical background motivates the use of microwave photons as long-range couplers between distant spin qubits, as discussed below (see also Ref. 28).

To fully exploit quantum computational power, a common strategy is to build a distributed quantum computing architecture with modules interconnected by long-range couplers.[29,30] These prospects echo the additional criteria regarding "flying qubits" proposed by DiVincenzo. Circuit cavity quantum electrodynamics provides an elegant framework for realizing flying qubits in the form of microwave photons.[2] These photons are confined as stationary electromagnetic fields within superconducting resonators. The real or virtual photons in the cavity can in principle distribute entanglement over larger distances and faster than other long-range coupling approaches such as directly shuttling charge carriers.[30] The building block of coherent couplings between a spin and a harmonic oscillator, namely, the microwave resonator, is the familiar Jaynes–Cummings Hamiltonian,[2]

$$H/\hbar = \omega_r a^+ a + \frac{1}{2}\omega_s \sigma_z + g(\sigma^+ a + \sigma^- a^+).$$

The first term describes a harmonic oscillator of resonance frequency ω_r, a^+ (a, respectively) being the creation (annihilation, respectively) operator. Throughout this review, we keep this (+) notation for creation operators of a photon. The second term describes a spin of resonance frequency ω_s, σ_z being a Pauli-z operator. The last term describes the coupling between the harmonic oscillator and the spin, where σ^+ and σ^- are the raising and lowering operators acting on the spin. Considering only a single excitation in the coupled system, at the resonant condition ($\omega_r = \omega_s$), the coupling between the spin and the harmonic oscillator yields new maximally entangled eigenstates, energetically separated by $2\hbar g$. The strong-coupling regime is characterized by a coupling strength that is much larger than the photon and spin decay rates.[21–27] In this regime, the excitation is allowed to be periodically transferred between the spin and the resonator for many times before being dissipated into the environment.

As mentioned earlier, a spin couples to the magnetic component of the electromagnetic field generated by the resonator with a typical strength of only a few hertz and is essentially insensitive to the resonator's electric field.[33] To circumvent this difficulty, a double quantum-dot (DQD) structure such as the one represented in Fig. 1(a) can be utilized to equip the spin qubit with an enhanced charge dipole moment.[31,33–36]

31 October 2026 16:32:36

© Author(s) 2026

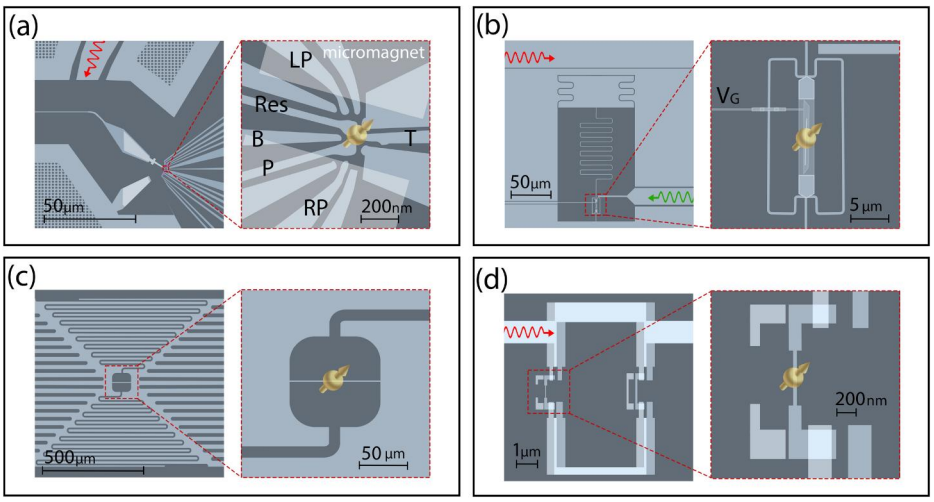

FIG. 1. Possible coupling schemes between single spins and a superconducting circuit (a) Semiconductor quantum-dot spin coupled to a microwave resonator through spin-charge hybridization, here enabled by a magnetic-field gradient. (b) Andreev spin qubit in a superconducting weak link, where the spin state modifies the phase-dependent Andreev spectrum and therefore the Josephson admittance of the circuit. (c) Rare-earth spin magnetically coupled to a superconducting resonator; in the bad-cavity regime, Purcell-enhanced emission can be detected using a single-microwave-photon detector. (d) Bismuth donor in silicon magnetically coupled to a superconducting flux qubit, whose large current fluctuations enhance the local vacuum magnetic field at the spin position.

When a single charge is confined in a double quantum dot (DQD) with a sufficiently large tunnel coupling rate t_c, the charge states corresponding to the electron being in the left dot ($|L\rangle$) or in the right dot ($|R\rangle$) can form a superposition when the two dots are energetically degenerate [see Figs. 2(a) and 2(b)]. This results in two hybridized eigenstates $(|L\rangle \pm |R\rangle)/\sqrt{2}$ separated by an energy splitting $2\hbar t_c$, forming the basis states of a "charge qubit" [Fig. 2(c)]. For electrons in silicon quantum dots, this configuration naturally produces a charge dipole of approximately 100 nm—much larger than the few picometers of a tightly bound electron in a single dot—allowing rapid switching between strong charge–photon coupling [see Fig. 2(d)] and nearly zero coupling.[31,37]

To further enhance the charge–photon coupling rate, it is important to use a resonator with a high characteristic impedance Z_r. For an electric-dipole coupling, the coupling strength is proportional to the voltage quantum fluctuations in the resonator, which scale as $\sqrt{Z_r}$ at fixed frequency. Increasing the resonator impedance therefore increases the vacuum electric field seen by the charge dipole of the double quantum dot. This should be contrasted with magnetic-dipole coupling, discussed in Sec. IV, where the coupling is proportional to the current quantum fluctuations, which scale as $1/\sqrt{Z_r}$. Low-impedance resonators are therefore advantageous for magnetic coupling, whereas high-impedance resonators are advantageous for electric coupling. For example, high impedance can be achieved by fabricating resonators from superconducting materials with high kinetic inductance.[38] High impedances of 1–4 kΩ have been demonstrated with these designs and used to enhance the charge–photon coupling strength. Following this approach, the impedance can be further increased by employing more "disordered" superconducting materials, such as granular aluminum, reaching values up to 100 kΩ.[39,40] An alternative method to obtain resonators with a high characteristic impedance is based on SQUID arrays.[41,42] High-impedance resonators can significantly enhance the charge–photon coupling strength. However, increasing the resonator impedance also introduces stronger Kerr nonlinearities, which can limit the cavity quality factor. In addition, the large gate electrodes of the dots create microwave leakage channels, further reducing the quality factor. To mitigate these effects and preserve cavity performance, on-chip gate filters are integrated in the gate fan-out region to block signal leakage.[33,43]

In materials with strong intrinsic spin–orbit interaction, such as electrons in III–V semiconductors or holes in silicon and germanium, the electron spin naturally couples to its orbital motion. In a double quantum dot (DQD), this coupling allows the spin state to become correlated with the electron position.[44] This intrinsic spin–orbit route is therefore one way to generate an effective electric dipole for the spin degree of freedom. In contrast, electrons in silicon, one of the most widely studied platforms, lack significant intrinsic spin–orbit interaction,[45] so the spin and charge degrees of freedom remain largely decoupled. To engineer a similar spin–charge hybridization, lithographically patterned micro- or nano-magnets are used to produce a transverse magnetic field gradient across the DQD. This gradient encodes the spin information into the electron's position, effectively realizing a synthetic spin–orbit interaction.[46,47] A spin qubit can therefore indirectly couple to a photon through a charge qubit.[31,34] To suppress charge noise, the charge qubit frequency is usually far detuned from both the spin qubit frequency, i.e., the Zeeman splitting, and the cavity frequency, so the charge degree of freedom only acts as a perturbation term in the spin–photon coupling.[25,44]

The first evidence of coherent spin–photon coupling was demonstrated in a carbon nanotube DQD with the help of ferromagnetic materials, but the coupling strength $g/2\pi = 1.3$ MHz remained smaller than the spin decay rate (2.5 MHz).[24,35] Two later experiments in silicon DQDs[31,34] report a strong spin–photon coupling strength of around ten megahertz compared to a cavity decay rate comprised

31 October 2026 16:32:36

© Author(s) 2026

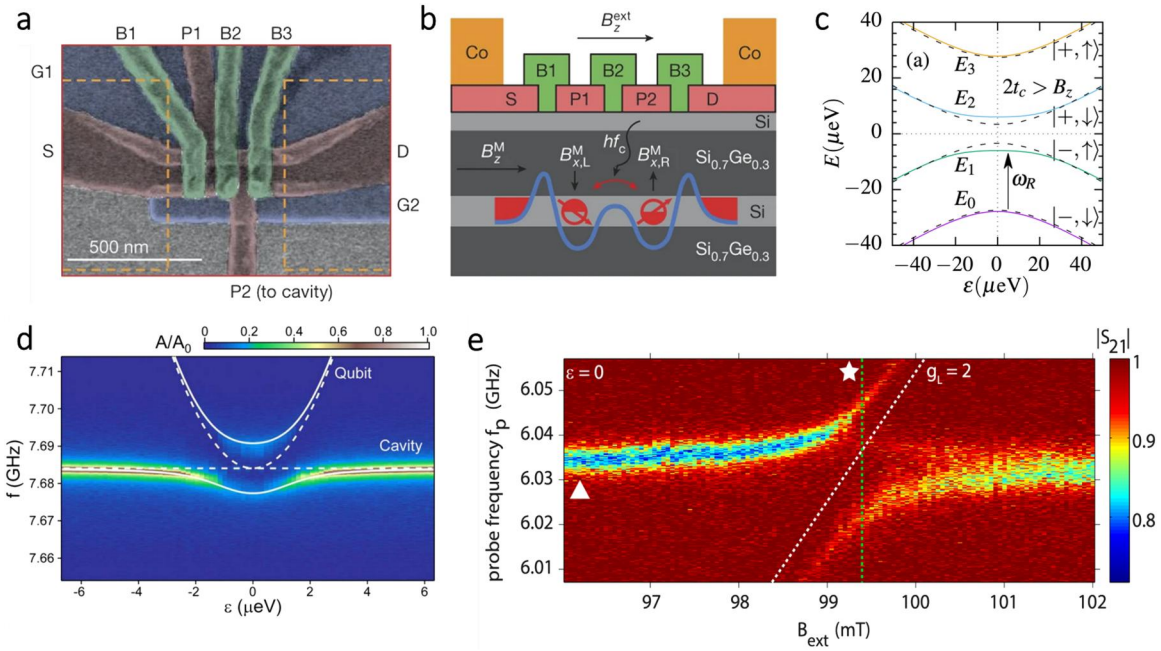

FIG. 2. (a) SEM image of a DQD with one of its plunger gates (P2) connected to the cavity. Orange dashed lines indicate the profile of a pair of Co magnets. (b) Layout of the substrate materials and the metallic gates. The DQD provides sufficient dipole moment for a single electron. The Co pair generates a local magnetic field with gradients in both the x and z axes, where the x-gradient hybridizes the spin and charge degrees of freedom. (c) The spin-charge hybridized energy levels. The lowest two levels E0 and E1 define the qubit basis states in the flopping-mode. The extra anti-crossing between E_1 and E_2 further bends their energy curvature, and thus hybridizes the spin and charge states. (d) Spectroscopy of the strong coupling between a charge qubit and a cavity. Due to its hyperbolic curvature, the charge qubit energy minimizes at zero detuning where the charge and the cavity maximally hybridize. (e) Spectroscopy of the strong coupling between a spin qubit and a cavity. The spin frequency linearly depends on the external magnetic field B_{ext}, yielding an avoided-crossing in the transmission signal |S21| used to probe the cavity. Panels (a) and (b) are adapted from Ref. 31. Panel (c) is adapted from Ref. 32. Panel (d) is adapted from Ref. 33. Panel (e) is adapted from Ref. 34.

between 1 and 5 MHz and a spin dephasing rate of around 2.5 MHz, as shown in Fig. 2(e). These experiments therefore entered the strong-coupling regime in the sense that g exceeded the dominant linewidths by a factor of a few. The first experiment used a resonator impedance of 200–300 Ω and a charge qubit linewidth of about 40 MHz, requiring the charge qubit to be set closer to the spin and photon in frequency, with a detuning of 1.55 GHz. The second experiment, although still limited by a charge qubit linewidth of 52 MHz, employs a high-impedance NbTiN resonator making it possible to achieve the strong spin–photon coupling regime with the charge qubit detuned by 6.45 GHz.

In a more recent experiment, a single-hole spin confined in a silicon-on-insulator (SOI) double quantum dot was coupled to a photon in a high-impedance NbN resonator with a strength of 330 MHz.[50] In addition to the strong intrinsic spin–orbit interaction of hole states, the large coupling strength is attributed to a large gate lever arm, $\alpha_g = 0.607$, reaching values up to 0.92 in a similar device. This is enabled by the thin and high-k dielectric layer between the hole and the gate, in comparison to a typical value of 0.1–0.2 in SiGe heterostructures.[51,52]

For qubits encoded in more than one spin, such as singlet-triplet qubits in a double dot and exchange-only qubits in a triple dot, strong spin–photon coupling can be achieved in the absence of intrinsic or synthetic spin–orbit interaction, because the cavity electric field can modulate the detuning or exchange interaction, thereby changing the qubit energy splitting and producing an effective electric-dipole coupling.[53] An experiment performed in a GaAs triple dot showed that an exchange-only qubit can strongly couple to a high-impedance NbTiN resonator with a strength of 31.4 MHz.[36] Later, a singlet-triplet qubit in an InAs nanowire was shown to couple to a NbTiN resonator with 139 MHz.[54] However, in this experiment, a strong intrinsic spin–orbit interaction is present and plays an important role for the qubit defined by the S(2,0) and T+(1,1) states.

When a cavity is coupled to two distant qubits through a common resonator mode, the spin–photon couplings can be used for coherent quantum state transfer between spatially separated qubits [see Fig. 3(a)], providing a basic building block for long-range connectivity in spin-qubit systems.[55,56] The Jaynes–Cummings Hamiltonian can be simply modified into the Tavis–Cummings Hamiltonian to describe such a system with more than one qubit. When the cavity is resonant with both qubits simultaneously $(\omega_r = \omega_{s1} = \omega_{s2})$, the system is in the Tavis–Cummings resonant regime. The collective vacuum Rabi splitting is enhanced by $\sqrt{N}$ for N identical qubits [see Figs. 3(b) and 3(c)]. In the experiments of Refs. 48 and 49, two spins were coupled to the same cavity mode, leading to the expected $\sqrt{2}$ enhancement of the collective coupling. An alternative configuration is to make the qubits resonant with each other but largely detuned from the cavity with $\Delta_i = |\omega_{si} - \omega_r| \gg g$. In this dispersive regime, virtual photons mediate an effective exchange coupling $J = g_1 g_2/\Delta$ (for equal detuning).[57] This idea connects directly

31 October 2026 16:32:36

© Author(s) 2026

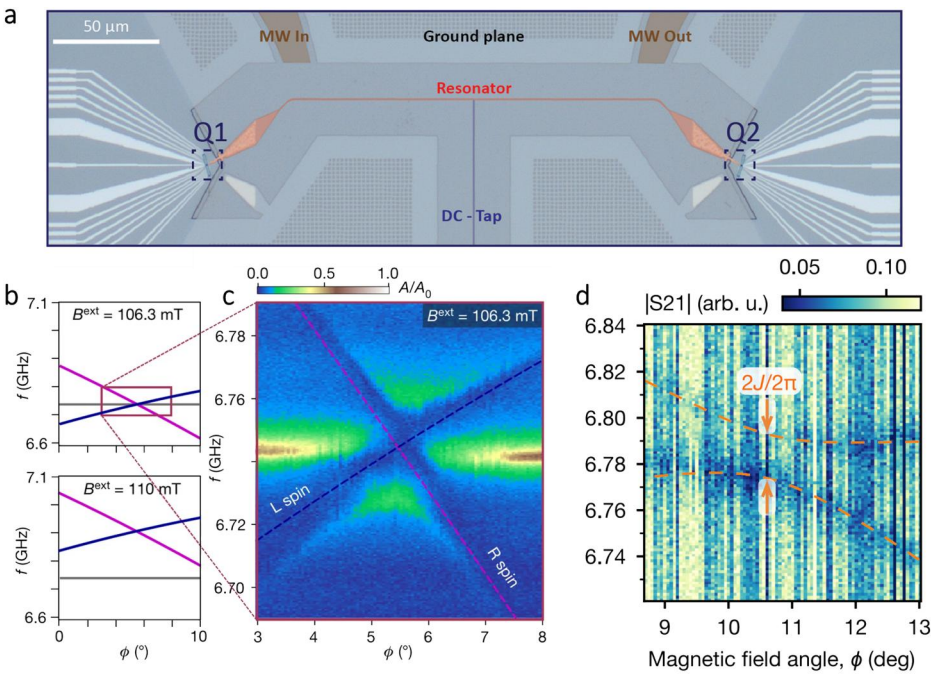

FIG. 3. (a) Optical microscope image of a device with a high-impedance NbTiN resonator and two DQDs sitting at the two ends of the resonator. Two spin qubits (Q1 and Q2) are hosted in the two DQDs, respectively. (b) Spin frequencies under two different magnetic fields. The upper panel shows the condition that two spins resonate with the cavity simultaneously. The lower panel shows the two spins resonate with each other while being significantly detuned from the cavity, known as spin–spin dispersive coupling. (c) The cavity transmission signal shows two spins strongly couple to the cavity at the same time [as in the upper panel in (b)], showing an enhanced vacuum Rabi splitting. (d) The cavity transmission signal shows the avoided-crossing of two distant spins that are dispersively coupled to each other via virtual photons [as in the lower panel in (b)]. Panel (a) is adapted from Ref. 29. Panels (b) and (c) are adapted from Ref. 48. Panel (d) is adapted from Ref. 49.

to early proposals for cavity-mediated interactions between distant spin qubits.[21,22] A dispersive spin–spin coupling with a strength tunable in the range of 30–60 MHz has been reported,[49] as shown in Fig. 3(d). It is worth noting that the cavity mediation can also couple heterogeneous qubits that lack a direct interaction mechanism, e.g., between a semiconductor spin qubit and a superconducting transmon qubit, making it possible to photonically network quantum computers built from different platforms.[58]

A. Time-domain

The spin-cavity hybrid system only becomes interesting for quantum information processing when the interaction can be controlled in real time. Two complementary regimes can be distinguished: resonant spin–photon exchange and dispersive spin–spin coupling mediated by virtual photons. In both cases, the key to time-domain control is to rapidly switch on and off the interaction between a qubit and the cavity. As discussed earlier, this can be done by pulsing the qubit between the flopping-mode regime and the localized mode regime.[31,37] For dispersive coupling, two distant qubits are simultaneously pulsed to the flopping-mode regime. These conditions lead to a dispersive spin–spin interaction mediated by virtual photons in the cavity. Precise control of the interaction time yields a coherent iSWAP-type gate. In a recent experiment, coherent oscillations were observed between two spin qubits separated by 250 μm[29] [see Figs. 4(a) and 4(b)]. With a high-impedance NbTiN coplanar cavity, an exchange oscillation frequency of 11–21 MHz is reported and demonstrated to be controllable by several knobs including the spin–photon frequency detuning and the DQD's tunnel coupling, matching well the theoretical predictions. Coherent quantum state transfer can also be implemented in the strong coupling regime. Here, the two qubits are sequentially instead of simultaneously brought into a resonant interaction with the cavity.[55] When strong spin–photon coupling is achieved, this leads to coherent vacuum Rabi oscillations in the time-domain with frequency $2g$, which have recently been reported experimentally in this platform.[59] Also the coherent transfer of an excitation from one spin to the other via a photon was achieved [see Figs. 4(c) and 4(d)]. Finally, a vacuum Rabi oscillation of one spin was used to prepare the cavity in a Fock state with one photon, after which the vacuum Rabi oscillation of the other spin was accelerated,[59] as expected.[60]

B. Longitudinal coupling

The conventional Jaynes–Cummings Hamiltonian describes the transverse coupling between a qubit and a cavity. It is also interesting to engineer a longitudinal coupling $H_c = g\sigma_z(a + a^+)$, which does not exchange energy between the qubit and the cavity. Instead, the cavity field is displaced in a way that depends on the qubit state, while the resonator quadrature shifts the qubit energy through the σ_z term.[27,61] For a single-spin qubit, the micromagnet must be designed to provide a large magnetic field difference along the longitudinal instead of the transverse direction with respect to the spin quantization axis. Under an external drive of the qubit near the cavity frequency, the cavity is conditionally excited depending on the qubit state. If another qubit at a distance is coupled to the cavity in a similar manner, its frequency can then be controlled by the cavity excitation and is therefore eventually conditioned on the state of the first qubit.[61] This effectively performs a controlled-phase (CPHASE) gate on the two distant qubits, similar to the geometric CPHASE gate between two nuclear spins mediated by driving a shared electron spin,[62] as discussed below in Sec. IV. A single-spin implementation has not yet been reported in experiment, but initial results have been obtained in an analogous setting with a singlet-triplet qubit.[63] A main advantage

31 October 2026 16:32:36

© Author(s) 2026

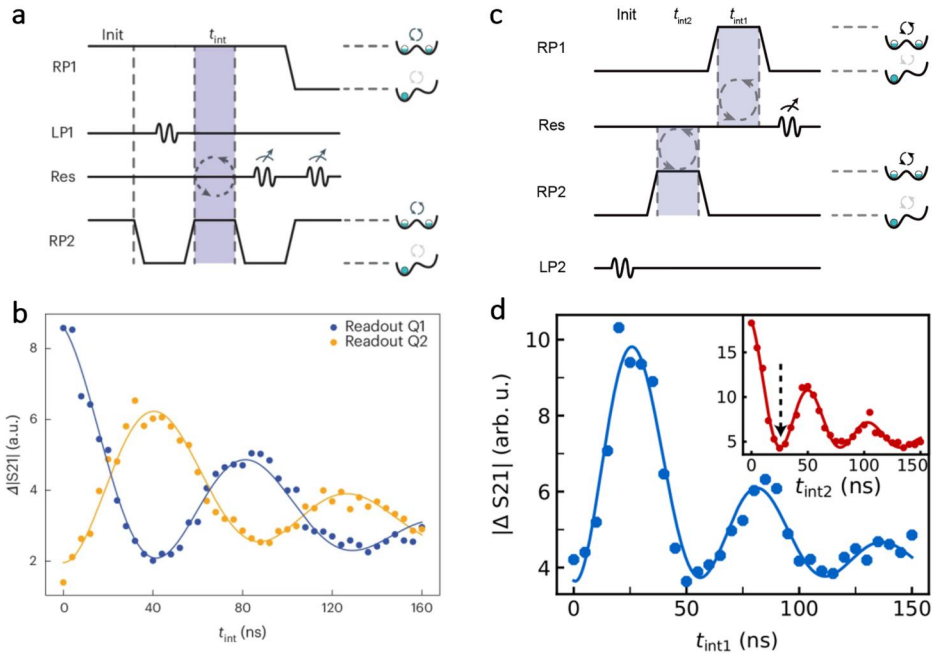

FIG. 4. (a) Pulse sequence used to probe iSWAP oscillation between two distant spins that are dispersively coupled to each other. RP1 and RP2 are pulsed to bring Q1 and Q2 in and out of the flopping-mode. A microwave burst applied to LP1 is used to initialize Q1 into the excited state. (b) Measured cavity transmission signals |S21| showing iSWAP oscillation between the two spin qubits. (c) Pulse sequence used to transfer an excitation from Q2 to Q1 by concatenating vacuum Rabi oscillations of each qubit with the cavity. A microwave burst is applied to LP2 to prepare Q2 in the excited state, followed by pulses on RP2 and RP1 to bring Q2 and Q1 into resonance with the cavity one by one. (d) Inset: |S21| signal showing vacuum Rabi oscillation with Q2 starting in the excited state and cavity empty. Main panel: |S21| signal showing vacuum Rabi oscillation with Q1 in the ground state and cavity populated by a photon emitted by Q2. Panel (a) and (b) are adapted from Ref. 29. Panel (c) and (d) are adapted from Ref. 59.

here is that the conditional cavity excitation can be simply provided by Pauli spin blockade and micromagnets are no longer necessary. A similar experiment has also been performed in a spin hybrid qubit, which utilizes the (2,1)–(1,2) transition in a DQD.[64] Noticeably, in this experiment, the cavity is placed on a separate chip and connected to the spin qubit via flip-chip technology, pointing to a promising direction of spin-cavity integration in the future. While a longitudinal two-qubit gate remains to be demonstrated, we can foresee several benefits such as that the qubits do not have to be resonant anymore and they can be far detuned from the cavity to mitigate the Purcell effect.[65,66]

C. Other application: Fast readout

Spin qubit readout is another important application of the spin-cavity hybrid system. Traditional spin readout is done by mapping the spin state onto a charge state, either through spin-selective tunneling to a reservoir[67,68] or using the Pauli spin blockade effect, making use of another reference spin.[69] Both approaches rely on a nearby sensing quantum dot whose conductance is capacitively dependent on the charge occupation in the dots to read. However, the drawbacks of using such charge sensors are clear: they rely on reservoirs of electrons or holes and can only sense qubits that are close-by. Circuit QED provides an elegant alternative to charge sensors by directly connecting the cavity galvanically to the dot electrodes, as discussed previously. Not only can this architecture read out multiple qubits in a frequency-multiplexed manner, but the high internal quality factor Q_i (internal loss rate $\kappa_i = \omega_r/Q_i$) also allows an enhancement in the sensitivity, thus resulting in an improved speed and accuracy. The readout speed is also set by the external quality factor Q_C (external coupling rate $\kappa_C = \omega_r/Q_C$) between the cavity and the feed line. For fast readout, one typically works with an over-coupled resonator ($Q_C \ll Q_i$), or equivalently ($\kappa_C \gg \kappa_i$), so that photons enter and leave the cavity rapidly through the measurement port. This contrasts with coherent spin–photon coupling experiments, where reducing the total cavity linewidth is usually more important and the external coupling is chosen more weakly in order to keep photons in the cavity for longer times.[70]

As discussed above, in the dispersive regime, QND readout of the spin qubit state can be implemented by probing the frequency shift of the cavity.[29,33] Here, the readout performance depends on the dispersive shift and therefore a large spin–photon coupling rate is desired. The sensitivity can be greatly enhanced by combining Pauli spin blockade with resonator-based reflectometry, known as gate-based readout.[71] Similar to the longitudinal coupling experiment, the singlet-triplet basis provides a dramatic conditional frequency change of the cavity, because it effectively turns the spin-dependence into charge-dependence. The charge-photon coupling rate g_c is usually several times larger than the spin–photon coupling rate g, giving rise to a visible improvement in the readout signal. An early experiment reports a single-shot readout of a spin qubit in natural silicon with a fidelity of 98% in only 6 μs.[72] As g_c is dominated by the gate lever

31 October 2026 16:32:36

© Author(s) 2026

arm, devices with thin dielectric layers are favorable for gate-based readout. In an experiment where a DQD made in SOI was studied, the readout cavity was patterned on a separate chip and wire-bonded to the DQD chip. Even with a significant parasitic capacitance that degrades the readout quality, a charge readout signal-to-noise ratio of 3.3 in only 50 ns was achieved, assisted by a remarkably large gate lever arm of 0.72.[52] With improved spin coherence in isotopically purified silicon and the implementation of a travelling-wave parametric amplifier, we are reasonably optimistic that this readout scheme could meet the requirements for rapid feedback control within the timescale of coherence and quantum error correction in real-time.

III. ANDREEV SPIN QUBITS

Andreev spin qubits (ASQs) encode quantum information in the spin of a single quasiparticle trapped in Andreev bound states (ABS) of a Josephson weak link. In comparison to the quantum dots discussed in Sec. II, the quasi-particles are confined not only by electrostatic fields but also by Andreev reflections at the superconductor–semiconductor interface. More precisely, the qubit is defined in the odd-parity manifold of the weak link: one unpaired quasiparticle occupies an Andreev level, and its two spin states form the qubit subspace. This distinguishes the ASQ from even-parity Andreev excitations, which correspond to pair-like transitions rather than to a single trapped spin. The basic concept of encoding and manipulating a qubit in the spin subspace of Andreev bound states was introduced by Chtchelkatchev and Nazarov.[73] Unlike conventional semiconductor spin qubits, ASQs couple to superconducting circuits through the spin-dependent supercurrent carried by the ABS [see Fig. 1(b)]. Equivalently, the spin state changes the phase-dependent Andreev energy $E_\sigma(\phi)$ of the weak link; since the supercurrent and Josephson admittance are determined by the phase dependence of this energy, the surrounding circuit becomes sensitive to the spin state. This direct spin-to-supercurrent interaction is enabled by the spin–orbit coupling of the weak link and yields strong, electrically tunable coupling to microwave resonators and superconducting qubits.[74–77] From the circuit perspective, this means that the spin state modifies the phase-dependent Andreev spectrum of the weak link, which appears to the surrounding superconducting circuit as a spin-dependent Josephson response. In the following, we review four recently explored topics: (i) spin spectroscopy of Andreev spectra, (ii) single-spin manipulation and dispersive readout, (iii) strong coupling to a superconducting transmon qubit, and (iv) long-range strong spin–spin interactions.

In proximitized semiconductor nanowires with strong Rashba spin–orbit interaction, discrete ABS form inside the superconducting gap. While many material platforms have been used to realize ABS, we will here focus primarily on superconductor-normal-superconductor (SNS) junctions defined in InAs nanowires covered with epitaxial aluminum.[78,79] A single trapped quasiparticle in the SNS junction has a spin degree of freedom that modulates the Josephson current across the junction. This provides the microscopic origin of the spin-dependent Josephson response introduced above. Embedding the device in a microwave cavity or a superconducting transmon qubit enables dispersive readout and coherent control.[77,80,81] In this configuration, the microwave circuit does not merely provide a drive or a readout resonator; it directly senses the spin-dependent admittance of the weak link. This is the basis for both dispersive readout and strong coupling to superconducting modes.

Before discussing coherent manipulation of Andreev spin qubits, it is useful to first recall how microwave spectroscopy reveals the spin structure of Andreev bound states. These measurements probe the phase-dependent excitation spectrum of the weak link and distinguish transitions associated with even-parity pair excitations from transitions within the odd-parity spin manifold.[82] They therefore provide the spectroscopic basis for identifying a trapped quasiparticle spin as a controllable two-level system. In Ref. 83, microwave spectroscopy resolved spin–orbit-split Andreev levels as characteristic bundles of phase-dispersing lines, revealing the internal spin structure of the weak link. Subsequent experiments identified two-quasiparticle singlet–triplet manifolds and showed how spin–orbit interaction mixes spin states,[84] allowing electrically driven spin flips even at high magnetic fields as shown in Fig. 5. In the odd-parity regime relevant for ASQs, the spectrum contains transitions between the two spin states of a single trapped quasiparticle; resolving these transitions is the key step that turns an Andreev level from a spectroscopic object into a spin-qubit degree of freedom.[85,86] These measurements built on circuit-QED techniques tailored to weak links.[77]

Once spin-resolved Andreev transitions have been identified spectroscopically, they can be used as controllable two-level systems. In this regime, the microwave circuit plays two roles: it can drive transitions within the Andreev spectrum, and it can read out the spin state through the state-dependent Josephson response of the weak link. The first coherent control of an ASQ was demonstrated in InAs/Al nanowires coupled to a superconducting resonator.[87] Raman transitions drove spin flips between ABS states, while the state-dependent Josephson inductance enabled dispersive single-shot readout.[88] Single-shot readout was critical because the SNS junction ground state was a singlet with no trapped quasiparticle; coherent spin manipulation therefore required post-selection on the odd-parity state, see Figs. 6(a) and 6(b). In Ref. 81, the use of additional barrier gates under the SNS junction enabled the doublet state, with a spin degree of freedom, to be the ground state of the SNS junction, making coherent manipulation more direct. The ASQ was operated in a ground-state doublet encoding, achieving all-electric Rabi frequencies exceeding 200 MHz with tunability over ∼10 GHz.

Direct strong coupling of an ASQ to a superconducting transmon was also demonstrated in Ref. 81. An avoided crossing with the transmon revealed coherent exchange with strength $2J/2\pi = 104$ MHz, see Figs. 6(c)–6(f). The coupling J exceeded both the ASQ decoherence rate and transmon linewidth, firmly establishing the strong-coupling regime.

Beyond single-qubit control and ASQ–transmon hybridization, the spin-dependent Josephson response can also mediate interactions between two Andreev spin qubits. Since each ASQ modifies the superconducting inductance of the circuit in a spin-dependent way, two spatially separated ASQs can interact through a common superconducting phase variable. In Ref. 89, two distant ASQs embedded in a double-loop SQUID were coupled via their shared Josephson inductance. The effective Hamiltonian corresponds to two spins coupled via an Ising-like ZZ interaction. In this experiment, this ZZ interaction reached up to 178 MHz, see Figs. 6(g)–6(j), tunable by gate voltages and flux, and switchable *in situ*.

Having demonstrated spectroscopy, coherent control, and strong coupling, the next key question is what limits ASQ coherence. This is a particularly important issue because the spin is embedded in a

31 October 2026 16:32:36

© Author(s) 2026

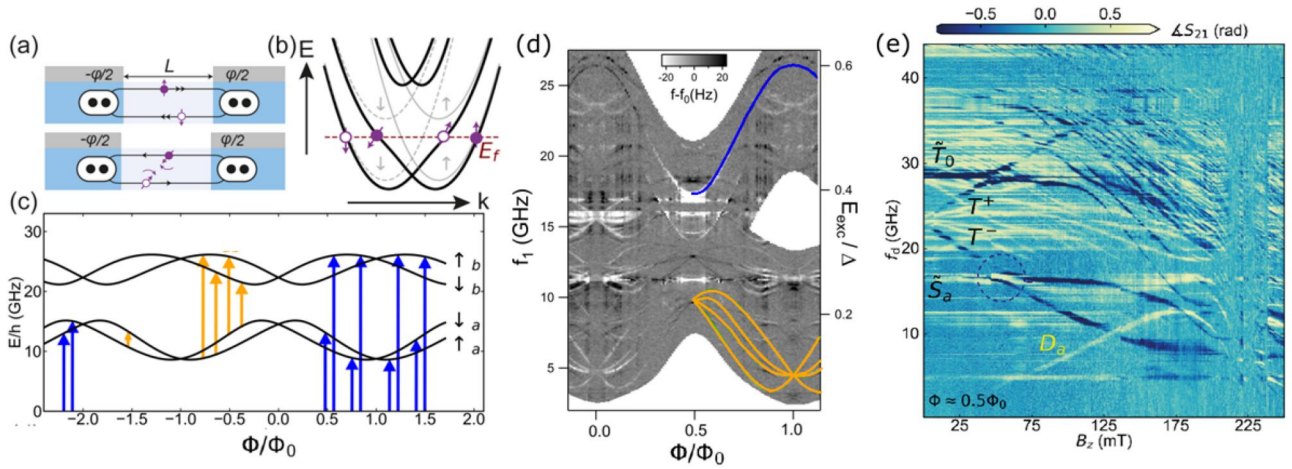

FIG. 5. (a) and (b) Schematic of a Josephson weak link hosting spinful Andreev bound states with phase-dependent energies $E(\varphi)$. In the presence of spin–orbit coupling and magnetic field, the spin degeneracy of the Andreev spectrum is lifted, so that odd-parity states with a single trapped quasiparticle form spin-resolved Andreev doublets. Importantly, the spin of these Andreev doublets couples strongly to the supercurrent across the junction. (c) Representative many-body spectrum showing even-parity pair excitations (blue) and odd-parity spin excitations (yellow) derived from the underlying Andreev levels. Microwave spectroscopy can access both pair-breaking transitions and transitions within the odd-parity manifold, thereby probing the internal spin degree of freedom of a trapped quasiparticle. (d) From Ref. 83, measured excitation spectrum as a function of superconducting phase difference together with calculated transition branches. The observation of several phase-dispersing resonances reflects the presence of multiple Andreev levels, as expected when the weak link extends beyond the short-junction limit. (e) From Ref. 84, field-resolved microwave spectroscopy of the Andreev spectrum. Besides the phase- and field-dependent pair transitions (labeled $\tilde{S}$ and $\tilde{T}$ for the singlet and triplet transitions), the resonance labeled D_a identifies a direct spin transition within a single odd-parity Andreev doublet, corresponding to a microwave-driven transition between the two Zeeman- and spin–orbit-split states of one trapped quasiparticle. Its direct observation demonstrates that the spin degree of freedom of an Andreev bound state can be spectroscopically resolved and coherently addressed. Panels (a), (b), (c), and (e) are reproduced from Ref. 84 and panel (d) is reproduced from Ref. 83.

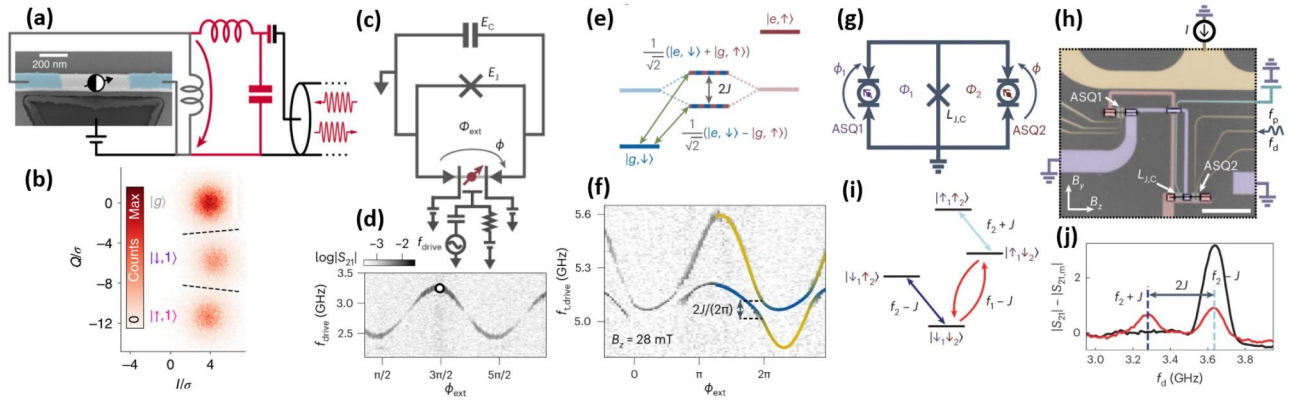

FIG. 6. (a) Device concept from Ref. 88 for dispersive readout of an Andreev spin qubit (ASQ): a semiconductor–superconductor Josephson weak link is embedded in a microwave circuit so that the spin-dependent supercurrent shifts the resonance of a superconducting resonator, enabling spin-to-photon conversion in circuit QED. (b) Single-shot measurement histogram of the resonator response, showing well-resolved measurement outcomes associated with the spin states and the ground-state configuration. The clear separation of the distributions demonstrates that the strong spin coupling to the resonator enables single-shot readout of the Andreev spin qubit states. (c) Circuit schematic of an ASQ coupled to a transmon from Ref. 81, with the flux-biased Josephson element providing phase control of the Andreev spectrum and the transmon. (d) Flux-dependent spectroscopy of the coupled device, where the observed resonance follows the phase dependence of the ASQ transition and demonstrates microwave addressability of the ASQ state in the hybrid spin-transmon architecture. (e) Level diagram of the hybridized ASQ-transmon system. Near resonance, the spin excitation and the transmon excitation mix into dressed states split by $2J$, evidencing coherent exchange between the two subsystems. (f) Measured avoided crossing between the ASQ and transmon as a function of flux, providing direct spectroscopic evidence of strong coupling between the spin and the transmon. The vacuum-Rabi-type splitting $2J$ is indicated in the figure. (g) Circuit layout of Ref. 89 for two distant ASQs coupled through a common transmon bus, which mediates an interaction between the spin-dependent supercurrents of the two junctions and allows the effective interqubit coupling to be tuned by flux. (h) Micrograph of the implemented two-ASQ device, showing the two Andreev spin qubits, the central coupling element, and the microwave feedline used for spectroscopy and control. (i) Effective level scheme for the two-spin manifold, illustrating how the transmon-mediated interaction shifts the transition frequencies separated by the coupling strength $2J$. (j) Two-spin spectroscopy displaying the split resonances $f_2 \pm J$, which directly reveal the strong longitudinal coupling between the two spins as mediated by the transmon. Panels (a) and (b) adapted from Ref. 88. Panels (c)–(f) adapted from Ref. 81. Panels (g)–(j) adapted from Ref. 89.

31 October 2026 16:32:36

© Author(s) 2026

superconducting weak link and can therefore be affected by both semiconductor and superconducting noise channels. In the first coherent-manipulation experiments, the spin lifetime and coherence were still far from those of isolated semiconductor spins; for example, a spin-flip time ($T_S = 17\,\mu$s) and an echo coherence time ($T_{2E} = 52$ ns) were reported in the excited-state ASQ encoding.[87] These values illustrate both the promise of fast circuit-QED readout and the present limitation imposed by parity dynamics, quasiparticle relaxation, and dephasing in the weak link. A recent analysis by Hoffman and coworkers treats electric- and magnetic-noise dephasing in Rashba nanowire-based ASQs and identifies magnetic noise from the nuclear spin bath of InAs as the dominant noise source,[90] which also hints toward the fact that materials with low nuclear spin yet still large spin–orbit interaction, such as Ge, could be a potentially better material for ASQ coherence. Exchange-driven and Knight-shift-like effects in dot-Josephson systems provide additional spectroscopic fingerprints[86,91] that may be helpful for future studies of ASQs.

ASQs have rapidly developed into a platform offering single-spin control, spin-resolved spectroscopy, strong coupling to superconducting qubits, and long-range ZZ interactions. Their hybrid character makes them promising candidates for scalable quantum processors and nanoscale probes of correlated states. Future work will focus on extending coherence[90] and scaling multi-ASQ networks,[92] with particular emphasis on parity stability, quasiparticle dynamics, and operation at coherence-protected working points.

IV. SPIN-RESONATOR MAGNETIC COUPLING

The most natural way to couple spins and superconducting circuits is via the magnetic dipole interaction. Although this interaction is weaker than electric-dipole coupling in quantum-dot systems or spin-dependent-supercurrent coupling in ASQs, there are good motivations to address spins magnetically. First, it is applicable to a large family of spin systems, since all spins have a magnetic dipole. Second, from the point of view of quantum computing, hybridizing spin and charge degrees of freedom (as needed for electrical coupling) may lead to an enhanced sensitivity to charge noise, and thus possibly to a lower coherence time.

This section considers the simplest superconducting circuit: a resonator, of frequency ω_r, coupled magnetically to a spin located in the vicinity of its inductance [see Fig. 1(c)]. The magnetic coupling between an electron spin of frequency ω_s and this resonator can be written as

$$\mathcal{H}_c = \vec{S} \cdot \gamma_e \cdot \delta\vec{B}(a + a^+),$$

where $\vec{S}$ is the spin operator, γ_e is the electronic gyromagnetic tensor, and $\delta\vec{B}$ is the rms fluctuations of the magnetic field component of the microwave field at the spin location.[93] In the rotating-wave approximation, this Hamiltonian can be re-written in a Jaynes–Cummings form, $H_c = \hbar g(\sigma^+ a + \sigma^- a^+)$. Typical values of electronic gyromagnetic ratio are close to the free-space value of 28 GHz T^{-1}. For typical resonator frequencies (in the 5–10 GHz), typical resonator designs (based on coplanar waveguides, or inter-digitated capacitors), and typical spin-resonator distance of 100 nm, values of $\delta B \sim 100$ nT can be obtained, yielding coupling constants 1–10 kHz at most[93] (Larger values can be obtained by using flux qubits, see Sec. V). This range of values is significantly smaller than the typical linewidth of a planar superconducting resonator, $\kappa/2\pi \sim 100$–500 kHz in the presence of a ~ 400 mT magnetic field needed to tune the spins at the resonator frequency. Therefore, it remains a challenging task to reach the strong magnetic coupling regime between a single spin of linewidth ~ 10–100 kHz, and a resonator.

While strong coupling is desirable for quantum information processing applications, it is however not a requirement. Recent experiments have operated in the so-called "bad-cavity regime," $g \leq \kappa$, where the cavity linewidth is larger than the single-spin coupling strength and coherent vacuum Rabi oscillations are not resolved. In this regime, the main impact of the cavity on the spin dynamics is via the Purcell effect, which enhances the spin radiative relaxation rate when the spin is at resonance, and channels the emitted microwave spontaneous emission into the output coaxial cable, via the resonator mode.[65,94] Here, the relevant figure of merit is not coherent exchange, but the Purcell-enhanced radiative rate into the resonator output channel, together with the efficiency and dark-count rate of the microwave-photon detector. When this radiative decay channel is sufficiently efficient compared with other spin-relaxation channels, the spin can be detected by counting the microwave photons emitted by Purcell-enhanced spontaneous emission. The electron spin ancilla can then be used in order to coherently drive and read out a small nuclear-spin qubit register coupled to it by the hyperfine interaction. This detection scheme requires to operate at millikelvin temperatures in order to minimize thermal excitation of the electron spin and suppress the number of thermal photons. It also relies on the use of a single microwave photon detector (SMPD), which remains an active area of research.

Several SMPD designs have recently been proposed and demonstrated, based on circuit-QED architectures.[95–98] Here, we will focus on one particular design,[99] which was used to demonstrate single-spin detection in recent experiments. The device relies on a four-wave-mixing process to map the presence (or absence) of a microwave photon at its input onto the state of a superconducting transmon qubit. The SMPD is operated cyclically, so that long time traces can be recorded. Its efficiency is maximum at the frequency of its input resonator within a detection bandwidth that can be tuned between 100 kHz and 1 MHz and should be approximately matched to the emitter linewidth for optimal sensitivity. The input frequency can be tuned to the frequency of the spin resonator to optimally detect the emitted photons. Efficiencies between 0.5 and 0.8, and dark-count rates in the 50–100 s^{-1} can be reached, sufficient for single-spin detection.[100–102]

The detection scheme was initially applied to the detection of an ensemble of electron spin donors in silicon.[103] It was then applied for spectroscopy of a scheelite crystal of $CaWO_4$, a tetragonal crystal whose unit cell is shown in Fig. 7(b).[104,105] $CaWO_4$ is a favorable matrix for spin qubits, because its constituents have predominantly zero nuclear-spin isotopes.[106] The main nuclear-spin isotope is ^{183}W, a spin-$\frac{1}{2}$ isotope with 14% natural abundance, a low magnetic moment of ($0.12\,\mu_N$), and a gyromagnetic ratio of 1.8 MHz T^{-1}. Among the many paramagnetic impurities in $CaWO_4$, Er^{3+} stands out as a particularly interesting one. It is a Kramers ion, behaving as an effective electron spin-1/2 at temperatures below 10 K with an axially symmetric gyromagnetic tensor, whose principal values are 17.45 GHz T^{-1} if the field is applied parallel to the axis, or 117.3 GHz T^{-1} if it is applied perpendicular to it. This large transverse gyromagnetic ratio leads to a correspondingly large coupling constant g, and therefore an enhanced radiative rate Γ_R.

31 October 2026 16:32:36

© Author(s) 2026

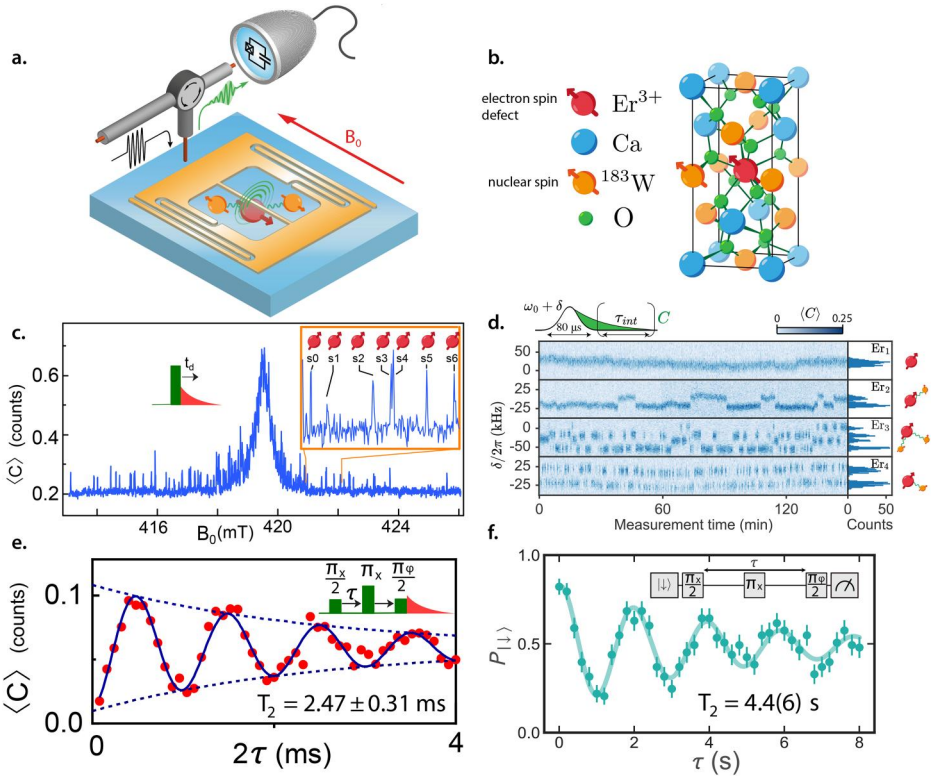

FIG. 7. (a) Single-spin ESR by microwave-photon counting, method. The electron spin (in red), biased by a dc magnetic field B_0, is coupled magnetically to a planar microwave resonator, fabricated out of a superconducting thin-film (in orange). The spin is excited by an incoming microwave pulse (in black), and relaxes radiatively by emitting a microwave photon (in green) into the detection waveguide, which is directed to the input of a microwave-photon counter based on a transmon qubit. (b) The electron spins are Er^{3+} doped into a crystal of $CaWO_4$, whose unit cell is displayed. Er substitutes for Ca. The main nuclear-spin species in $CaWO_4$ arises from the 14%-abundant spin-1/2 ^{183}W isotope of tungsten. (c) Single-spin-resolved Er^{3+}:$CaWO_4$ spectroscopy. The number of counts, $\langle C\rangle$, is shown as a function of B_0 amplitude, applied approximately along the crystalline c axis. The 1 mT-broad peak is signal from the Er^{3+} spin ensemble. Narrow peaks are from individual Er^{3+} spins. (d) Time traces of the Er^{3+} spin resonance for four different spins. The number of counts $\langle C\rangle$ is shown as a function of δ, the detuning of the exciting microwave pulse from the resonator frequency ω_r. Er_1 shows no resolved quantum jump, Er_2 and Er_4 show quantum jumps due to one strongly coupled ^{183}W nuclear spin, and Er_3 shows quantum jumps due to two strongly coupled ^{183}W nuclear spins. (e) Hahn-echo signal of one Er^{3+} spin. The phase of the third pulse relative to the first two is set as $\phi = 2\omega_I\tau$, with $\omega_I/2\pi = 1$ kHz, resulting in an oscillating echo signal. The signal is exponentially damped with a characteristic time $T_2 = 2.5$ ms, limited by the electron spin relaxation. (f) Hahn-echo signal of one ^{183}W nuclear spin. The phase of the third pulse is also set to $\phi = 2\omega_I\tau$, explaining the oscillating echo signal. The decay is exponential, with a time constant $T_2 = 4.4$ s.

Figure 7(a) summarizes the experiment. At a temperature of 10 mK, and an operating frequency of 7.5 GHz, the Er^{3+} spins are fully polarized in their ground state at thermal equilibrium. A microwave pulse at ω_r is sent to the spin resonator input and excites the spins, which then relax radiatively at a rate Γ_R, emitting toward an SMPD placed after a coaxial cable. The number of detected SMPD clicks, C, was recorded over an appropriately chosen integration time. Repeating the experiment yields the ensemble-averaged number of counts $\langle C\rangle$, shown in Fig. 7(c) as a function of the applied magnetic field. A millitesla-wide ensemble peak is observed at the field 419.5 mT corresponding to the expected Er^{3+} resonance in this field condition. Around this peak, much narrower peaks are observed, corresponding to emission from individual Er^{3+} spins.[107] The photon counting traces show an exponential decay of the emission when the field is tuned to one of these peaks,[107] with a typical emission rate of $1000\,s^{-1}$. Intensity–intensity correlations[107] display clear anti-bunching, providing evidence that the emission originates from individual spins. In view of possible quantum computing applications, the coherence time was measured with a Hahn-echo pulse sequence applied to various ions. Typical values around 2 ms were measured [see Fig. 7(e)], limited by the relaxation time, 1 ms.[107] These long coherence times confirm the interest of $CaWO_4$ as a host for spin qubits.

Further studies[108] have probed the nuclear-spin environment of various individual Er^{3+} ions. To this end, the magnetic field was set at an Er^{3+} peak, and high-resolution spectroscopy of the Er^{3+} spin was performed over 150 minutes. Results are shown in Fig. 7(d) for four different ions, labeled Er1–Er4. Three of them show well-resolved frequency jumps, indicative of their coupling to neighboring ^{183}W nuclear spins.

The coupled Er^{3+}–^{183}W nuclear-spin system is described by the Hamiltonian $H/\hbar = \omega_S S_z + \omega_I I_z + S_z(A_\parallel I_z + A_\perp I_x)$. In this equation, the Er^{3+} effective spin-1/2 is described by the spin operators $S_{x,y,z}$, z being the Er^{3+} quantization axis (which may differ from the direction of the applied magnetic field if the field is not aligned along

31 October 2026 16:32:36

© Author(s) 2026

one of the crystalline axes, due to the anisotropy of the gyromagnetic tensor). The ^{183}W nuclear spin, of Larmor frequency ω_I, is described by the spin operators $I_{x,y,z}$, z being here the magnetic field direction. The hyperfine coupling is due to the dipolar interaction between the two magnetic moments; it includes the longitudinal term $A_\parallel$ and the transverse term $A_\perp$, both of which are much smaller than the ^{183}W Larmor frequency ω_I in the applied field of 420 mT. In that limit, the eigenstates are well approximated by the uncoupled states ordered by increasing energy as $|\downarrow\Uparrow\rangle, |\downarrow\Downarrow\rangle, |\uparrow\Uparrow\rangle, |\uparrow\Downarrow\rangle$), where the first arrow describes the Er^{3+} spin, and the second one the ^{183}W state. Nuclear-spin-preserving transitions are EPR-allowed. Their transition frequency is $\omega_S \pm A_\parallel/2$. Nuclear-spin-flipping transitions (zero and double quantum), occurring at $\omega_S \pm \omega_I$, are only weakly allowed (so-called "forbidden"), due to the transverse hyperfine term, $A_\perp/2$.

This simple level structure explains the time traces shown in Fig. 7(d). The microwave pulse excites the Er^{3+} spin on an allowed transition, after which it relaxes radiatively to its ground state. This relaxation occurs with a high probability on the same allowed transition, in which case the Er^{3+} frequency will not change in the next sequence. However, there is a small probability that the Er^{3+} spin relaxes on a forbidden transition, causing the nuclear spin to change its state, and therefore the allowed transition frequency of the next sequence to shift by $A_\parallel$, which is manifested by a sudden jump in the time traces. Similar nuclear-spin quantum jumps have been observed in a variety of contexts, using either optical[109] or electrical[110,111] detection of an electron spin ancilla.

Because the values of $A_\parallel$ and $A_\perp$ depend on the position of the ^{183}W with respect to the Er^{3+}, the frequency jump size and rate depend on the individual nuclear-spin configuration around the Er^{3+}, which is different for each atom because of the 14% abundance of this isotope. In particular, Er_1 has zero strongly coupled ^{183}W, Er_2 and Er_4 have one, and Er_3 has two. Note that each Er^{3+} is moreover coupled to an extended bath of many weakly coupled ^{183}W; their progressive reconfiguration in time explains for a large part the spectral diffusion observed in Fig. 7(d).

In order to use the ^{183}W nuclear spins as a qubit register, it is necessary to read out their state, initialize them in a well-defined state, and operate single- and two-qubit gates. These tasks are achieved via the Er^{3+} electron spin ancilla, in close analogy to the operation of ^{13}C nuclear-spin qubit register via a nitrogen-vacancy center in diamond.[112]

Nuclear state readout is achieved by applying repetitive pulses on one of the allowed transitions (say, the $|\downarrow\Uparrow\rangle$ to $|\uparrow\Uparrow\rangle$), and counting the subsequently emitted photons. $\langle C\rangle$ will be larger if the nuclear spin is in $|\Uparrow\rangle$ than in $|\Downarrow\rangle$, enabling single-shot readout in 100 ms.[108]

State preparation is achieved by microwave driving of a forbidden transition (say, from $|\downarrow\Uparrow\rangle$ to $|\uparrow\Downarrow\rangle$). If the nuclear spin is initially in $|\Downarrow\rangle$, the electron spin is not excited and the nuclear spin will remain in $|\Downarrow\rangle$. If the nuclear spin is initially in $|\Uparrow\rangle$, the pulse will flip it to $|\Downarrow\rangle$, while exciting the Er^{3+} spin, which will subsequently relax with high probability on the allowed transition, leaving the ^{183}W spin also in $|\Downarrow\rangle$.[108] Repeating this pulse therefore increases the probability to prepare the ^{183}W spin in $|\Downarrow\rangle$ at the end of the sequence, which can reach values close to unity.[108]

Single-qubit gates require driving the nuclear spins at their Larmor frequency, which is around 780 kHz at 450 mT. Applying radio frequency through a 7 GHz resonator at 10 mK is challenging because of signal filtering by the microwave resonator. Another possibility is to use microwave-stimulated Raman transitions. They consist of a pair of microwave pulses applied simultaneously and detuned by a frequency δ, with a frequency close to, but not resonant with, any of the electron spin transitions. When δ matches the resonance frequency of a given nuclear spin, the latter can then be driven via a second-order process in which the Er^{3+} spin is virtually excited.[113] Because the resonance frequency of each nuclear spin is $\omega_I - A_\parallel/2$ (when the Er^{3+} is in $|\downarrow\rangle$), which is different for every nuclear spin, the microwave Raman pulses enable coherent control of individual nuclear spins even in a small register. The ^{183}W nuclear-spin coherence time under a Hahn-echo pulse sequence is measured to be 4 s [see Fig. 7(f)]. Such long coherence times confirm that $CaWO_4$ is a good matrix for nuclear-spin qubits. Two-qubit gates can also be performed using conditional ac-Zeeman shifts under the microwave Raman drives.[113]

In order to move toward the development of a quantum computer architecture based on nuclear-spin qubits, two-qubit gates between Er^{3+} spins are required. Here again, the resonator could mediate the $Er^{3+} - Er^{3+}$ interaction. Recent work shows that resonator-mediated spin-spin interaction is compatible with dynamical decoupling, which raises hope that such task can be achieved in the near future.

V. FLUX QUBITS COUPLED TO IMPURITY DONORS

As mentioned earlier, direct magnetic coupling between a single electron spin and a conventional superconducting resonator is usually limited by the small vacuum current fluctuations of a linear microwave mode. In a harmonic oscillator, the zero-point current fluctuations scale, at fixed resonance frequency, as ($\delta I \propto 1/\sqrt{Z_r}$). Enhancing magnetic coupling with a linear resonator would therefore require using very low-impedance resonators. In practice, however, fabricating superconducting resonators with impedances far below ($\sim$10 Ω), while preserving good microwave properties is technically challenging. This makes the impedance of a linear resonator a practical limiting factor for magnetic spin–photon coupling.

A way around this limitation is to use a nonlinear superconducting circuit rather than a linear harmonic oscillator. In such a circuit, the potential energy is not restricted to a single quadratic minimum. It can instead develop two minima associated with opposite nonzero persistent currents. When these two current states are tuned into degeneracy, tunneling hybridizes them into eigenstates with zero average circulating current at the symmetry point. However, the current operator still has a large matrix element between the two eigenstates, or equivalently large quantum current fluctuations. These fluctuations are no longer limited by the harmonic-oscillator scaling ($\delta I \propto 1/\sqrt{Z_r}$), and can generate a much stronger local microwave magnetic field for coupling to nearby impurity spins.

Flux qubits provide a concrete implementation of this idea. They are nonlinear superconducting circuits formed by a loop interrupted by Josephson junctions, as illustrated in Fig. 8(a) for a four-junction device.[115–118] In the design considered here, the loop contains four junctions: three nominally identical junctions and a fourth junction smaller by a factor α. The origin of the double-well structure can be understood from the Josephson potential energy of the circuit. This potential is obtained by summing the Josephson energies of the junctions, with the superconducting phase drops constrained by flux quantization. For a loop containing $n-1$ identical junctions and one

31 October 2026 16:32:36

© Author(s) 2026

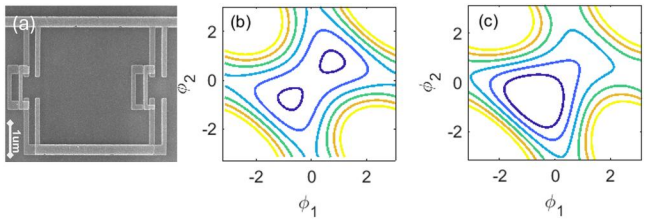

FIG. 8. (a) Scanning electron microscope (SEM) image of a four-junction flux qubit. Three of the junctions are identical while the fourth one is smaller than the others by a factor α. (b) and (c) Potential energy landscape of a three-junction flux qubit with $\alpha = 0.7$ for $\Phi/\varphi_0 = \pi$ (b) and $\Phi/\varphi_0 = 1.2\pi$ (c). Adapted from Ref. 114.

smaller junction of Josephson energy αE_J, threaded by an external dc magnetic flux Φ, one can write

$$U = -E_J\left[\sum_{i=1}^{n-1}\cos(\varphi_i) + \alpha\cos\left(\frac{\Phi}{\varphi_0} - \sum_{i=1}^{n-1}\varphi_i\right)\right],$$

where φ_i is the superconducting phase drop across the identical junctions, and $\varphi_0 = \hbar/2e$ is the reduced flux quantum. At the symmetry point $\Phi/\varphi_0 = \pi$, and for suitable values of α, this potential develops two degenerate minima, which correspond to two possible persistent-current states circulating in opposite directions. The two minima are separated by a central potential barrier located at $\varphi_i = 0$, and their positions are determined by the general condition

$$\sin\varphi^* = \alpha\sin[(n-1)\varphi^*].$$

This double-well structure is illustrated in Fig. 8(b) for a three-junction flux qubit with $\alpha = 0.7$ at $\Phi/\varphi_0 = \pi$. Away from the symmetry point, for example at $\Phi/\varphi_0 = 1.2\pi$, the degeneracy between the two potential minima is lifted, as shown in Fig. 8(c).

For the four-junction flux qubit shown in Fig. 8(a), the corresponding persistent currents are

$$I_P = \pm I_0\sin\varphi^* = \pm I_0\sqrt{\frac{3}{4} - \frac{1}{4\alpha}},$$

where I_0 is the critical current of the identical junctions. For typical junction parameters, this gives persistent currents of the order of 300–500 nA.

At the symmetry point, the two classical current states, denoted $|\circlearrowleft\rangle$ and $|\circlearrowright\rangle$, are degenerate. Tunneling through the central barrier hybridizes them into symmetric and antisymmetric superpositions, which form the two lowest-energy eigenstates of the flux qubit and are separated in energy by the tunnel splitting $\hbar\Delta$.[119] These eigenstates have zero average circulating current, but the current matrix element between them remains large, of order I_P. The corresponding quantum current fluctuations therefore generate an enhanced local microwave magnetic field for coupling to a nearby spin.[120–122] This enhancement had already been exploited to reach the strong-coupling regime at the ensemble level: Zhu *et al.* demonstrated a superconducting flux qubit coherently coupled to an ensemble of nitrogen-vacancy centers in diamond, resolving a clear vacuum-Rabi-type splitting in the qubit spectrum.[6] The single-donor experiment described below extends this same strategy—replacing a linear resonator by a flux qubit to boost the local magnetic vacuum fluctuations—from the ensemble down to the level of individual spins.

The Hamiltonian of the circuit can then be written as

$$\mathcal{H}_{qb} = \frac{\hbar}{2}\left(\Delta\sigma_{qb}^z + \varepsilon\sigma_{qb}^x\right),$$

where $\varepsilon = \frac{2I_p}{\hbar}(\Phi - \pi\varphi_0)$, and σ_{qb}^z and σ_{qb}^x are Pauli operators acting on the subspace formed by the ground and first excited eigenstates of the circuit Hamiltonian. It is important here to note two major issues related to flux-qubit design. The huge magnetic moment ($\sim$5 PHz T^{-1}), makes the energy of each level extremely sensitive to external magnetic fluctuations, except at the so-called optimal point $\Phi/\varphi_0 = \pi$ where the first-order sensitivity to flux noise vanishes.[116,123] Additionally, the tunneling rate $\Delta/2\pi$ depends exponentially on the parameters of the junctions,[119] generating a sizeable irreproducibility.[116–118,123] This problem has been recently partially mitigated by new fabrication techniques allowing an extremely good control of e-beam lithography, oxidation parameters of the junctions and sample surface treatment.[124,125]

In a recent work,[126] a flux qubit was used to couple to individual bismuth donors. One of the advantages of bismuth donors is their large hyperfine coupling constant, which gives rise to an electron spin resonance transition at 7.377 GHz without applying an external magnetic field.[65,127] They can be implanted near the surface with good yield and low straggling[128] and possess long coherence times.[129,130]

In order to make a coherent exchange, the flux-qubit frequency must be tuned in resonance with the spins. This condition was achieved in Ref. 126 by dressing the flux qubit with a resonant drive. When the amplitude of the drive is equal to the detuning between the qubit and the spin, it is possible to show that a time-independent flip-flop interaction takes place between the two systems.[122]

Figure 9(a) illustrates the protocol used to detect individual spins with the driven flux qubit. To distinguish bismuth donors from random environmental spins or two-level systems, the measurement is repeated after a waiting time. Only spins whose state is preserved over this delay contribute to the difference between the two readouts. Since bismuth donors in silicon are known to exhibit very long relaxation times,[65] this memory effect provides a way to identify them among other microscopic defects in the environment. Once a donor spin has been identified, the driven flux qubit can be brought into resonance with it in the dressed frame, allowing coherent excitation exchange. The resulting swap oscillations, shown in Fig. 9(b), provide access to the spin–qubit coupling strength and to the spin coherence properties.

The coupling strength between the flux qubit and the bismuth donor is found to reach $g/2\pi = 84$ kHz. The flux qubit used in this work has a relaxation time of $T_1 \sim 5\,\mu$s and is dressed by a resonant drive with an amplitude of order 100 MHz to bring it into resonance with the bismuth donor. Under this continuous drive, the dominant dephasing mechanism of the undriven qubit, 1/f flux noise,[116–118] is efficiently filtered out, and its contribution becomes negligible compared with relaxation.[131] The dressed qubit can therefore be characterized by an effective decoherence time approximately equal to $\frac{4}{3}T_1$. We therefore use gT_1 as the relevant figure of merit, obtaining $gT_1 \sim 3$, which currently places the system close to the threshold of the strong-coupling regime. While this value limits the fidelity of a SWAP operation, realistic improvements could increase this figure of merit up to $gT_1 \sim 40$ by both moderately increasing the critical

31 October 2026 16:32:36

© Author(s) 2026

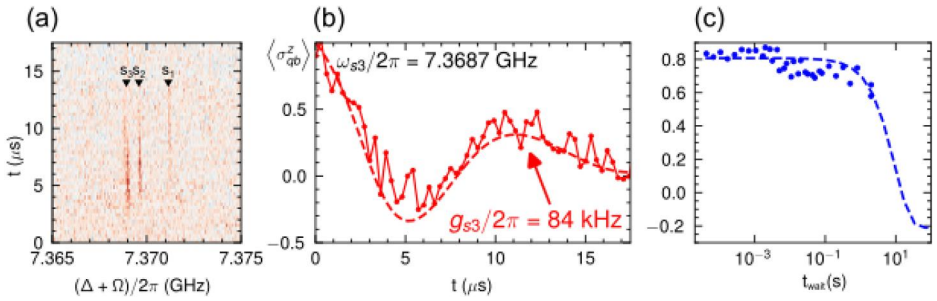

FIG. 9. (a) Qubit state difference vs Rabi frequency (Ω) and interaction time (t) after two successive readouts. Only spins with a relaxation time longer than the elapsed time between the two readouts are visible. Three Si:Bi donors are detected at $\omega_{s1}/2\pi = 7.3712$ GHz, $\omega_{s2}/2\pi = 7.3692$ GHz, and $\omega_{s3}/2\pi = 7.3687$ GHz. (b) Coherent oscillations between the driven flux qubit and spin 3. The dashed lines are the results of a Lindblad simulation giving $g/2\pi = 84$ kHz. (c) Measurement of the qubit state $\langle \sigma^z_{qb} \rangle$ vs waiting time t_{wait} between SWAP protocols showing a spin relaxation time longer than 10 s. Panels (a)–(c) are adapted from Ref. 126.

current of the junctions from 300 nA to ≳600 nA and improving the relaxation times up to 40 μs as recently shown in Ref. 125. The relaxation time of the spin can be extracted by measuring the qubit state after successive SWAP protocols [see Fig. 9(c)]. This time is very long as expected (>10 s).

This experiment shows that flux qubits can overcome the small magnetic dipole coupling of individual donor spins by replacing the weak zero-point current fluctuations of a linear resonator with the much larger current fluctuations of a nonlinear superconducting circuit. The price paid is that the spin may inherit some of the limitations of the superconducting qubit, in particular its relaxation and dephasing. Future progress will therefore depend on improving flux-qubit coherence, increasing the persistent current and field confinement, and developing pulse protocols that enable high-fidelity spin control without sacrificing the long intrinsic coherence of the donor.

To advance toward spin-based quantum computing architectures, the realization of high-fidelity single- and two-qubit gate operations is essential. Such gates may be implemented using more sophisticated pulse schemes, thereby paving the way for a new generation of hybrid quantum processors. Using similar techniques, a range of further experiments could be extended to other donor species, such as tellurium impurities.[132] Compared with bismuth, tellurium may offer the additional advantage of activating donor spins closer to the silicon surface, where magnetic coupling to the flux qubit is strongest. Another promising research direction is the manipulation and exploitation of the rich nuclear-spin manifold of bismuth donors.[133]

VI. CONCLUSIONS

The concept of coupling individual spins to superconducting circuits has developed into several experimentally distinct architectures. These approaches should not be viewed simply as competing implementations of the same idea, but rather as different solutions to the same basic problem: how to overcome the very weak magnetic interaction between a single spin and a microwave circuit while preserving the advantages of the spin degree of freedom. Each platform realizes a different compromise between coupling strength, coherence, tunability, readout efficiency, and circuit-induced back-action.

Semiconductor quantum-dot spins achieve large effective spin–photon coupling strengths by converting spin dynamics into an effective electric-dipole moment through spin–charge hybridization, either engineered with micromagnets or provided intrinsically by spin–orbit interaction. This approach benefits from gate tunability, high-impedance resonators, and compatibility with scalable semiconductor devices. In addition to mediating long-range interactions between distant spins, coupling a spin qubit to a microwave cavity can also facilitate fast, high-fidelity, and potentially multiplexed single-shot readout. The main challenge is that the same electric-dipole character that enhances the coupling also exposes the spin to charge noise and cavity-induced relaxation.

Andreev spin qubits offer a different route in which a spin degree of freedom couples to a superconducting phase degree of freedom through a spin-dependent supercurrent. This mechanism naturally produces large and electrically tunable interactions with superconducting resonators or transmons, but the main challenges are now to improve coherence, stabilize parity, and control quasiparticle dynamics.

Direct magnetic coupling remains weaker, but it preserves the microscopic spin degree of freedom without requiring spin–charge hybridization. In this regime, the superconducting circuit can act as a quantum-limited measurement interface rather than only as a coherent bus. Purcell-enhanced emission combined with single-microwave-photon detection has made it possible to detect and study individual spins, opening a path toward nanoscale magnetic resonance and nuclear-spin registers.

Flux qubits provide yet another way to enhance magnetic coupling by using large current fluctuations in a nonlinear superconducting circuit. This approach is particularly attractive for donor spins with long intrinsic coherence and rich hyperfine structure. Its performance is currently limited by the coherence of the superconducting element, but improvements in flux-qubit design could directly translate into higher-fidelity spin–circuit operations.

Table I summarizes these four approaches in terms of their dominant coupling channel and representative energy scales. It highlights an important point: no single figure of merit is sufficient to rank the different platforms. Large coupling strengths are essential for fast gates and coherent exchange, but linewidths, tunability, noise sensitivity, compatibility with the magnetic fields required by the spin system, and the intended function of the circuit—bus, detector, or control element—are equally important. In the table, γ denotes a representative spin linewidth or decoherence

31 October 2026 16:32:36

© Author(s) 2026

TABLE I. Comparison of coupling schemes between single spins and superconducting circuits.

Superconducting circuit	Spin system	Dominant coupling channel	$\gamma/2\pi$	$\kappa/2\pi$	$g/2\pi$
High-impedance resonator	Electron/hole spin in double quantum dots	Electrical dipoles spin-charge hybridization	2–3 MHz	1–5 MHz	10–40 MHz
Superconducting resonator and transmon	Andreev spin qubit	Spin-dependent supercurrent	≈10 MHz	1–5 MHz	≳100 MHz
Low-impedance resonator + SMPD	Er^{3+} in CaWO4	Magnetic dipole Purcell-enhanced emission	∼5 kHz	100–500 kHz	1–10 kHz
Superconducting flux qubits	Si:Bi donor	Magnetic dipole-enhanced current fluctuations	1 Hz–1 kHz	20–100 kHz	50–200 kHz

rate, κ the superconducting-circuit linewidth, and g the spin–circuit coupling strength.

Taken together, these results show that coupling single spins to superconducting circuits is no longer a single-platform challenge, but a broader design problem in hybrid quantum engineering. The next milestones are likely to differ across platforms: coherent long-range gates for quantum-dot and Andreev spin qubits, improved single-spin detection and nuclear-spin control for magnetic-resonator architectures, and higher-fidelity spin–flux-qubit swaps for donor systems. Across all approaches, progress will depend on improving the balance between coupling strength, coherence, measurement efficiency, magnetic-field compatibility, and circuit-induced back-action. Achieving this balance would move the field from demonstrations of coupling and spectroscopy toward more complete hybrid systems for quantum processing and nanoscale magnetic resonance.

ACKNOWLEDGMENTS

This work was supported by the Israeli Science Foundation under Grant No. Quantum ISF #2471/24 and by the Helen Diller Quantum Center at the Technion. C.K.A. acknowledges support from the European Innovation Council Pathfinder Grant No. 101115315 (QuKiT) and the Dutch Research Council (NWO) through the Talent Programme VIDI: VI.Vidi.233.031. L.M.K.V. acknowledges financial support from the Dutch Research Council (NWO) via the National Growth Fund program Quantum Delta NL (Grant No. NGF.1623.23.024), the Horizon Europe program of the European Union under Grant Agreement No. 101174557 (QLSI2), and by the Army Research Office (ARO) under Grant No. W911NF2310110. X.X. acknowledges financial support from the Dutch Research Council (NWO) via the National Growth Fund program Quantum Delta NL (Grant No. NGF.1623.23.024) and the National Natural Science Foundation of China (Grant No. 12674619). The views and conclusions contained in this document are those of the authors and should not be interpreted as representing the official policies, either expressed or implied, of the ARO or the U.S. Government. The U.S. Government is authorized to reproduce and distribute reprints for government purposes notwithstanding any copyright notation herein. This work benefited from a French government grant managed by the ANR agency under the "France 2030 plan," with reference ANR-22-PETQ-0003.

AUTHOR DECLARATIONS

Conflict of Interest

The authors have no conflicts to disclose.

Author Contributions

M. Stern: Conceptualization (equal); Formal analysis (equal); Investigation (equal); Methodology (equal); Supervision (equal); Validation (equal); Visualization (equal); Writing – original draft (equal); Writing – review & editing (equal). **X. Xue:** Conceptualization (equal); Formal analysis (equal); Investigation (equal); Methodology (equal); Supervision (equal); Validation (equal); Writing – original draft (equal); Writing – review & editing (equal). **E. Flurin:** Conceptualization (equal); Formal analysis (equal); Investigation (equal); Methodology (equal); Supervision (equal); Validation (equal); Writing – original draft (equal); Writing – review & editing (equal). **C. K. Andersen:** Conceptualization (equal); Formal analysis (equal); Investigation (equal); Methodology (equal); Supervision (equal); Validation (equal); Writing – original draft (equal); Writing – review & editing (equal). **L. M. K. Vandersypen:** Conceptualization (equal); Formal analysis (equal); Investigation (equal); Methodology (equal); Supervision (equal); Validation (equal); Writing – original draft (equal); Writing – review & editing (equal). **P. Bertet:** Conceptualization (equal); Formal analysis (equal); Investigation (equal); Methodology (equal); Supervision (equal); Validation (equal); Writing – original draft (equal); Writing – review & editing (equal).

DATA AVAILABILITY

The data that support the findings of this study are available within the article.

REFERENCES

[1]A. A. Clerk, M. H. Devoret, S. M. Girvin, F. Marquardt, and R. J. Schoelkopf, Rev. Mod. Phys. **82**, 1155 (2010).
[2]A. Blais, A. L. Grimsmo, S. M. Girvin, and A. Wallraff, Rev. Mod. Phys. **93**, 025005 (2021).

31 October 2026 16:32:36

© Author(s) 2026

[3]Y. Kubo, F. R. Ong, P. Bertet, D. Vion, V. Jacques, D. Zheng, A. Dréau, J.-F. Roch, A. Auffeves, F. Jelezko, J. Wrachtrup, M. F. Barthe, P. Bergonzo, and D. Esteve, Phys. Rev. Lett. **105**, 140502 (2010).
[4]D. I. Schuster, A. P. Sears, E. Ginossar, L. DiCarlo, L. Frunzio, J. J. L. Morton, H. Wu, G. A. D. Briggs, B. B. Buckley, D. D. Awschalom, and R. J. Schoelkopf, Phys. Rev. Lett. **105**, 140501 (2010).
[5]P. Bushev, A. K. Feofanov, H. Rotzinger, I. Protopopov, J. H. Cole, C. M. Wilson, G. Fischer, A. Lukashenko, and A. V. Ustinov, Phys. Rev. B **84**, 060501(R) (2011).
[6]X. Zhu, S. Saito, A. Kemp, K. Kakuyanagi, S-i Karimoto, H. Nakano, W. J. Munro, Y. Tokura, M. S. Everitt, K. Nemoto, M. Kasu, N. Mizuochi, and K. Semba, Nature **478**, 221–224 (2011).
[7]V. Ranjan, G. de Lange, R. Schutjens, T. Debelhoir, J. P. Groen, D. Szombati, D. J. Thoen, T. M. Klapwijk, R. Hanson, and L. DiCarlo, Phys. Rev. Lett. **110**, 067004 (2013).
[8]S. Probst, H. Rotzinger, S. Wünsch, P. Jung, M. Jerger, M. Siegel, A. V. Ustinov, and P. A. Bushev, Phys. Rev. Lett. **110**, 157001 (2013).
[9]A. Imamoğlu, Phys. Rev. Lett **102**, 083602 (2009).
[10]D. Loss and D. P. DiVincenzo, Phys. Rev. A **57**, 120 (1998).
[11]L. M. K. Vandersypen, H. Bluhm, J. S. Clarke, A. S. Dzurak, R. Ishihara, A. Morello, D. J. Reilly, L. R. Schreiber, and M. Veldhorst, npj Quantum Inf. **3**, 34 (2017).
[12]M. Veldhorst, J. C. C. Hwang, C. H. Yang, A. W. Leenstra, B. de Ronde, J. P. Dehollain, J. T. Muhonen, F. E. Hudson, K. M. Itoh, A. Morello, and A. S. Dzurak, Nat. Nanotechnol. **9**, 981–985 (2014).
[13]S. Neyens, O. K. Zietz, T. F. Watson, F. Luthi, A. Nethwewala, H. C. George, E. Henry, M. Islam, A. J. Wagner, F. Borjans, E. J. Connors, J. Corrigan, M. J. Curry, D. Keith, R. Kotlyar, L. F. Lampert, M. T. Mądzik, K. Millard, F. A. Mohiyaddin, S. Pellerano, R. Pillarisetty, M. Ramsey, R. Savytskyy, S. Schaal, G. Zheng, J. Ziegler, N. C. Bishop, S. Bojarski, J. Roberts, and J. S. Clarke, Nature **629**, 80–85 (2024).
[14]X. Xue, M. Russ, N. Samkharadze, B. Undseth, A. Sammak, G. Scappucci, and L. M. K. Vandersypen, Nature **601**, 343–347 (2022).
[15]A. Noiri, K. Takeda, T. Nakajima, T. Kobayashi, A. Sammak, G. Scappucci, and S. Tarucha, Nature **601**, 338–342 (2022).
[16]A. R. Mills, C. R. Guinn, M. J. Gullans, A. J. Sigillito, M. M. Feldman, E. Nielsen, and J. R. Petta, Sci. Adv. **8**, eabn5130 (2022).
[17]S. G. J. Philips, M. T. Mądzik, S. V. Amitonov, S. L. de Snoo, M. Russ, N. Kalhor, C. Volk, W. I. L. Lawrie, D. Brousse, L. Tryputen, B. P. Wuetz, A. Sammak, M. Veldhorst, G. Scappucci, and L. M. K. Vandersypen, Nature **609**, 919–924 (2022).
[18]F. Borsoi, N. W. Hendrickx, V. John, M. Meyer, S. Motz, F. van Riggelen, A. Sammak, S. L. de Snoo, G. Scappucci, and M. Veldhorst, Nat. Nanotechnol. **19**, 21–27 (2024).
[19]Members of the HRL Quantum Team and Collaborators, M. Abraham, E. Acuna, T. S. Adams *et al.*, "A digitally controlled silicon quantum processing unit," Nature **655**, 1154–1159 (2026).
[20]J. J. Dijkema, X. Zhang, A. Bardakas, D. Bouman, A. Cuzzocrea, D. van Driel, D. Girardi, L. E. A. Stehouwer, G. Scappucci, A. M. J. Zwerver, and N. W. Hendrickx, "Simultaneous operation an 18-qubit modular array germanium," arXiv:2604.01063 (2026).
[21]L. Childress, A. S. Sørensen, and M. D. Lukin, Phys. Rev. A **69**, 042302 (2004).
[22]G. Burkard and A. Imamoglu, Phys. Rev. B **74**, 041307(R) (2006).
[23]M. Trif, V. N. Golovach, and D. Loss, Phys. Rev. B **77**, 045434 (2008).
[24]A. Cottet and T. Kontos, Phys. Rev. Lett. **105**, 160502 (2010).
[25]X. Hu, Y-x Liu, and F. Nori, Phys. Rev. B **86**, 035314 (2012).
[26]C. Kloeffel, M. Trif, P. Stano, and D. Loss, Phys. Rev. B **88**, 241405(R) (2013).
[27]F. Beaudoin, D. Lachance-Quirion, W. A. Coish, and M. Pioro-Ladrière, Nanotechnology **27**, 464003 (2016).
[28]G. Burkard, M. J. Gullans, X. Mi, and J. R. Petta, Nat. Rev. Phys. **2**, 129–140 (2020).
[29]J. Dijkema, X. Xue, P. Harvey-Collard, M. Rimbach-Russ, S. L. de Snoo, G. Zheng, A. Sammak, G. Scappucci, and L. M. K. Vandersypen, Nat. Phys. **21**, 168–174 (2025).
[30]M. De Smet, Y. Matsumoto, A.-M. J. Zwerver, L. Tryputen, S. L. de Snoo, S. V. Amitonov, S. R. Katiraee-Far, A. Sammak, N. Samkharadze, O. Gül, R. N. M. Wasserman, E. Greplová, M. Rimbach-Russ, G. Scappucci, and L. M. K. Vandersypen, Nat. Nanotechnol. **20**, 866–872 (2025).
[31]X. Mi, M. Benito, S. Putz, D. M. Zajac, J. M. Taylor, G. Burkard, and J. R. Petta, Nature **555**, 599–603 (2018).
[32]M. Benito, X. Mi, J. M. Taylor, J. R. Petta, and G. Burkard, Phys. Rev. B **96**, 235434 (2017).
[33]X. Mi, J. V. Cady, D. M. Zajac, J. Stehlik, L. F. Edge, and J. R. Petta, Appl. Phys. Lett. **110**, 043502 (2017).
[34]N. Samkharadze, G. Zheng, N. Kalhor, D. Brousse, A. Sammak, U. C. Mendes, A. Blais, G. Scappucci, and L. M. K. Vandersypen, Science **359**, 1123–1127 (2018).
[35]J. J. Viennot, M. C. Dartiailh, A. Cottet, and T. Kontos, Science **349**, 408–411 (2015).
[36]A. J. Landig, J. V. Koski, P. Scarlino, U. C. Mendes, A. Blais, C. Reichl, W. Wegscheider, A. Wallraff, K. Ensslin, and T. Ihn, Nature **560**, 179–184 (2018).
[37]K. D. Petersson, L. W. McFaul, M. D. Schroer, M. Jung, J. M. Taylor, A. A. Houck, and J. R. Petta, Nature **490**, 380–383 (2012).
[38]N. Samkharadze, A. Bruno, P. Scarlino, G. Zheng, D. P. DiVincenzo, L. DiCarlo, and L. M. K. Vandersypen, Phys. Rev. Appl. **5**, 044004 (2016).
[39]M. Khorramshahi, M. Spiecker, P. Paluch, S. Geisert, N. Gosling, N. Zapata, L. Brauch, C. Kübel, S. Dehm, R. Krupke, W. Wernsdorfer, I. M. Pop, and T. Reisinger, Phys. Rev. Appl. **24**, 024066 (2025).
[40]C. Roy, S. Frasca, and P. Scarlino, "Study of magnetic field resilient high impedance high-kinetic inductance superconducting resonators," arXiv:2503.13321 (2025).
[41]N. A. Masluk, I. M. Pop, A. Kamal, Z. K. Minev, and M. H. Devoret, Phys. Rev. Lett. **109**, 137002 (2012).
[42]C. Altimiras, O. Parlavecchio, P. Joyez, D. Vion, P. Roche, D. Esteve, and F. Portier, Appl. Phys. Lett. **103**, 212601 (2013).
[43]P. Harvey-Collard, G. Zheng, J. Dijkema, N. Samkharadze, A. Sammak, G. Scappucci, and L. M. K. Vandersypen, Phys. Rev. Appl. **14**, 034025 (2020).
[44]M. Benito, X. Croot, C. Adelsberger, S. Putz, X. Mi, J. R. Petta, and G. Burkard, Phys. Rev. B **100**, 125430 (2019).
[45]F. A. Zwanenburg, A. S. Dzurak, A. Morello, M. Y. Simmons, L. C. L. Hollenberg, G. Klimeck, S. Rogge, S. N. Coppersmith, and M. A. Eriksson, Rev. Mod. Phys. **85**, 961 (2013).
[46]M. Pioro-Ladrière, T. Obata, Y. Tokura, Y.-S. Shin, T. Kubo, K. Yoshida, T. Taniyama, and S. Tarucha, Nat. Phys. **4**, 776–779 (2008).
[47]E. Kawakami, P. Scarlino, D. R. Ward, F. R. Braakman, D. E. Savage, M. G. Lagally, M. Friesen, S. N. Coppersmith, M. A. Eriksson, and L. M. K. Vandersypen, Nat. Nanotechnol. **9**, 666–670 (2014).
[48]F. Borjans, X. G. Croot, X. Mi, M. J. Gullans, and J. R. Petta, Nature **577**, 195–198 (2020).
[49]P. Harvey-Collard, J. Dijkema, G. Zheng, A. Sammak, G. Scappucci, and L. M. K. Vandersypen, Phys. Rev. X **12**, 021026 (2022).
[50]C. X. Yu, S. Zihlmann, J. C. Abadillo-Uriel, V. P. Michal, N. Rambal, H. Niebojewski, T. Bedecarrats, M. Vinet, É. Dumur, M. Filippone, B. Bertrand, S. De Franceschi, Y.-M. Niquet, and R. Maurand, Nat. Nanotechnol. **18**, 741–746 (2023).
[51]M. F. Gonzalez-Zalba, S. Barraud, A. J. Ferguson, and A. C. Betz, Nat. Commun. **6**, 6084 (2015).
[52]D. J. Ibberson, T. Lundberg, J. A. Haigh, L. Hutin, B. Bertrand, S. Barraud, C.-M. Lee, N. A. Stelmashenko, G. A. Oakes, L. Cochrane, J. W. Robinson, M. Vinet, M. F. Gonzalez-Zalba, and L. A. Ibberson, PRX Quantum **2**, 020315 (2021).
[53]V. Srinivasa, J. M. Taylor, and C. Tahan, Phys. Rev. B **94**, 205421 (2016).
[54]J. H. Ungerer, A. Pally, A. Kononov, S. Lehmann, J. Ridderbos, P. P. Potts, C. Thelander, K. A. Dick, V. F. Maisi, P. Scarlino, A. Baumgartner, and C. Schönenberger, Nat. Commun. **15**, 1068 (2024).
[55]M. A. Sillanpää, J. I. Park, and R. W. Simmonds, Nature **449**, 438–442 (2007).
[56]J. Majer, J. M. Chow, J. M. Gambetta, J. Koch, B. R. Johnson, J. A. Schreier, L. Frunzio, D. I. Schuster, A. A. Houck, A. Wallraff, A. Blais, M. H. Devoret, S. M. Girvin, and R. J. Schoelkopf, Nature **449**, 443–447 (2007).
[57]M. Benito, J. R. Petta, and G. Burkard, Phys. Rev. B **100**, 081412 (2019).

31 October 2026 16:32:36

© Author(s) 2026

[58]P. Scarlino, D. J. van Woerkom, U. C. Mendes, J. V. Koski, A. J. Landig, C. K. Andersen, S. Gasparinetti, C. Reichl, W. Wegscheider, K. Ensslin, T. Ihn, A. Blais, and A. Wallraff, Nat. Commun. **10**, 3011 (2019).
[59]X. Xue, J. Dijkema, T. Bonsen, P. Harvey-Collard, M. Rimbach-Russ, S. L. de Snoo, G. Zheng, A. Sammak, G. Scappucci, and L. M. K. Vandersypen, "Controllable interaction between photons and distant spins via vacuum Rabi oscillations," arXiv:2608.03809 (2026).
[60]M. Hofheinz, E. M. Weig, M. Ansmann, R. C. Bialczak, E. Lucero, M. Neeley, A. D. O'Connell, H. Wang, J. M. Martinis, and A. N. Cleland, Nature **454**, 310–314 (2008).
[61]S. Bosco, P. Scarlino, J. Klinovaja, and D. Loss, Phys. Rev. Lett. **129**, 066801 (2022).
[62]M. T. Mądzik, S. Asaad, A. Youssry, B. Joecker, K. M. Rudinger, E. Nielsen, K. C. Young, T. J. Proctor, A. D. Baczewski, A. Laucht, V. Schmitt, F. E. Hudson, K. M. Itoh, A. M. Jakob, B. C. Johnson, D. N. Jamieson, A. S. Dzurak, C. Ferrie, R. Blume-Kohout, and A. Morello, Nature **601**, 348–353 (2022).
[63]C. G. L. Bøttcher, S. P. Harvey, S. Fallahi, G. C. Gardner, M. J. Manfra, U. Vool, S. D. Bartlett, and A. Yacoby, Nat. Commun. **13**, 4773 (2022).
[64]J. Corrigan, B. Harpt, N. Holman, R. Ruskov, P. Marciniec, D. Rosenberg, D. Yost, R. Das, W. D. Oliver, R. McDermott, C. Tahan, M. Friesen, and M. Eriksson, Phys. Rev. Appl. **20**, 064005 (2023).
[65]A. Bienfait, J. J. Pla, Y. Kubo, X. Zhou, M. Stern, C. C. Lo, C. D. Weis, T. Schenkel, D. Vion, D. Esteve, J. J. L. Morton, and P. Bertet, Nature **531**, 74–77 (2016).
[66]L. Noirot, C. X. Yu, J. C. Abadillo-Uriel, É. Dumur, H. Niebojewski, B. Bertrand, R. Maurand, and S. Zihlmann, "Coherence of a hole spin flopping-mode qubit in a circuit quantum electrodynamics environment," Nat. Phys. **22**, 917–923 (2026).
[67]J. M. Elzerman, R. Hanson, L. H. Willems van Beveren, B. Witkamp, L. M. K. Vandersypen, and L. P. Kouwenhoven, Nature **430**, 431–435 (2004).
[68]A. Morello, J. J. Pla, F. A. Zwanenburg, K. W. Chan, K. Y. Tan, H. Huebl, M. Möttönen, C. D. Nugroho, C. Yang, J. A. van Donkelaar, A. D. C. Alves, D. N. Jamieson, C. C. Escott, L. C. L. Hollenberg, R. G. Clark, and A. S. Dzurak, Nature **467**, 687–691 (2010).
[69]J. R. Petta, A. C. Johnson, J. M. Taylor, E. A. Laird, A. Yacoby, M. D. Lukin, C. M. Marcus, M. P. Hanson, and A. C. Gossard, Science **309**, 2180–2184 (2005).
[70]M. Göppl, A. Fragner, M. Baur, R. Bianchetti, S. Filipp, J. M. Fink, P. J. Leek, G. Puebla, L. Steffen, and A. Wallraff, J. Appl. Phys. **104**, 113904 (2008).
[71]J. I. Colless, A. C. Mahoney, J. M. Hornibrook, A. C. Doherty, H. Lu, A. C. Gossard, and D. J. Reilly, Phys. Rev. Lett. **110**, 046805 (2013).
[72]G. Zheng, N. Samkharadze, M. L. Noordam, N. Kalhor, D. Brousse, A. Sammak, G. Scappucci, and L. M. K. Vandersypen, Nat. Nanotechnol. **14**, 742–746 (2019).
[73]N. M. Chtchelkatchev and Y. V. Nazarov, Phys. Rev. Lett. **90**, 226806 (2003).
[74]C. Padurariu and Y. V. Nazarov, Phys. Rev. B **81**, 144519 (2010).
[75]B. Béri, J. H. Bardarson, and C. W. J. Beenakker, Phys. Rev. B **77**, 045311 (2008).
[76]S. Park and A. L. Yeyati, Phys. Rev. B **96**, 125416 (2017).
[77]C. Metzger, S. Park, L. Tosi, C. Janvier, A. A. Reynoso, M. F. Goffman, C. Urbina, A. Levy Yeyati, and H. Pothier, Phys. Rev. Res. **3**, 013036 (2021).
[78]P. Krogstrup, N. L. B. Ziino, W. Chang, S. M. Albrecht, M. H. Madsen, E. Johnson, J. Nygård, C. M. Marcus, and T. S. Jespersen, Nat. Mater. **14**, 400–406 (2015).
[79]W. Chang, S. M. Albrecht, T. S. Jespersen, F. Kuemmeth, P. Krogstrup, J. Nygård, and C. M. Marcus, Nat. Nanotechnol. **10**, 232–236 (2015).
[80]M. Hays, G. de Lange, K. Serniak, D. J. van Woerkom, D. Bouman, P. Krogstrup, J. Nygård, A. Geresdi, and M. H. Devoret, Phys. Rev. Lett. **121**, 047001 (2018).
[81]M. Pita-Vidal, A. Bargerbos, R. Žitko, L. J. Splitthoff, L. Grünhaupt, J. J. Wesdorp, Y. Liu, L. P. Kouwenhoven, R. Aguado, B. van Heck, A. Kou, and C. K. Andersen, Nat. Phys. **19**, 1110–1115 (2023).
[82]C. Janvier, L. Tosi, L. Bretheau, u O. Girit, M. Stern, P. Bertet, P. Joyez, D. Vion, D. Esteve, M. F. Goffman, H. Pothier, and C. Urbina, Science **349**, 1199–1202 (2015).
[83]L. Tosi, C. Metzger, M. F. Goffman, C. Urbina, H. Pothier, S. Park, A. L. Yeyati, J. Nygård, and P. Krogstrup, Phys. Rev. X **9**, 011010 (2019).
[84]J. J. Wesdorp, F. J. Matute-Cañadas, A. Vaartjes, L. Grünhaupt, T. Laeven, S. Roelofs, L. J. Splitthoff, M. Pita-Vidal, A. Bargerbos, D. J. van Woerkom, P. Krogstrup, L. P. Kouwenhoven, C. K. Andersen, A. L. Yeyati, B. van Heck, and G. de Lange, Phys. Rev. B **109**, 045302 (2024).
[85]A. Bargerbos, M. Pita-Vidal, R. Žitko, J. Ávila, L. J. Splitthoff, L. Grünhaupt, J. J. Wesdorp, C. K. Andersen, Y. Liu, L. P. Kouwenhoven, R. Aguado, A. Kou, and B. van Heck, PRX Quantum **3**, 030311 (2022).
[86]A. Bargerbos, M. Pita-Vidal, R. Žitko, L. J. Splitthoff, L. Grünhaupt, J. J. Wesdorp, Y. Liu, L. P. Kouwenhoven, R. Aguado, C. K. Andersen, A. Kou, and B. van Heck, Phys. Rev. Lett. **131**, 097001 (2023).
[87]M. Hays, V. Fatemi, D. Bouman, J. Cerrillo, S. Diamond, K. Serniak, T. Connolly, P. Krogstrup, J. Nygård, A. Levy Yeyati, A. Geresdi, and M. H. Devoret, Science **373**, 430–433 (2021).
[88]M. Hays, V. Fatemi, K. Serniak, D. Bouman, S. Diamond, G. de Lange, P. Krogstrup, J. Nygård, A. Geresdi, and M. H. Devoret, Nat. Phys. **16**, 1103–1107 (2020).
[89]M. Pita-Vidal, J. J. Wesdorp, L. J. Splitthoff, A. Bargerbos, Y. Liu, L. P. Kouwenhoven, and C. K. Andersen, Nat. Phys. **20**, 1158–1163 (2024).
[90]S. Hoffman, M. Hays, K. Serniak, T. Hazard, and C. Tahan, Phys. Rev. B **111**, 045304 (2025).
[91]L. Pavešić, M. P. Vidal, A. Bargerbos, and R. Žitko, SciPost Phys. **15**, 070 (2023).
[92]M. Pita-Vidal, J. J. Wesdorp, and C. K. Andersen, PRX Quantum **6**, 010308 (2025).
[93]P. Haikka, Y. Kubo, A. Bienfait, P. Bertet, and K. Mølmer, Phys. Rev. A **95**, 022306 (2017).
[94]C. Eichler, A. J. Sigillito, S. A. Lyon, and J. R. Petta, Phys. Rev. Lett. **118**, 037701 (2017).
[95]Y.-F. Chen, D. Hover, S. Sendelbach, L. Maurer, S. T. Merkel, E. J. Pritchett, F. K. Wilhelm, and R. McDermott, Phys. Rev. Lett. **107**, 217401 (2011).
[96]K. Inomata, Z. Lin, K. Koshino, W. D. Oliver, J.-S. Tsai, T. Yamamoto, and Y. Nakamura, Nat. Commun. **7**, 12303 (2016).
[97]J.-C. Besse, S. Gasparinetti, M. C. Collodo, T. Walter, P. Kurpiers, M. Pechal, C. Eichler, and A. Wallraff, Phys. Rev. X **8**, 021003 (2018).
[98]S. Kono, K. Koshino, Y. Tabuchi, A. Noguchi, and Y. Nakamura, Nat. Phys. **14**, 546–549 (2018).
[99]R. Lescanne, S. Deléglise, E. Albertinale, U. Réglade, T. Capelle, E. Ivanov, T. Jacqmin, Z. Leghtas, and E. Flurin, Phys. Rev. X **10**, 021038 (2020).
[100]L. Balembois, J. Travesedo, L. Pallegoix, A. May, E. Billaud, M. Villiers, D. Estève, D. Vion, P. Bertet, and E. Flurin, Phys. Rev. Appl. **21**, 014043 (2024).
[101]L. Pallegoix, J. Travesedo, A. S. May, L. Balembois, D. Vion, P. Bertet, and E. Flurin, "Enhancing the sensitivity of single microwave photon detection with bandwidth tunability," Phys. Rev. Appl. **25**, 044064 (2026).
[102]A. S. May, L. Sutevski, J. Solard, G. Cardoso, L. Carde, L. Pallegoix, R. Lescanne, D. Vion, P. Bertet, and E. Flurin, "Noise mitigation in single microwave photon counting by cascaded quantum measurements," arXiv:2502.14804 (2025).
[103]E. Albertinale, L. Balembois, E. Billaud, V. Ranjan, D. Flanigan, T. Schenkel, D. Estève, D. Vion, P. Bertet, and E. Flurin, Nature **600**, 434–438 (2021).
[104]E. Billaud, L. Balembois, M. Le Dantec, M. Rančić, E. Albertinale, S. Bertaina, T. Chanelière, P. Goldner, D. Estève, D. Vion, P. Bertet, and E. Flurin, Phys. Rev. Lett. **131**, 100804 (2023).
[105]E. Billaud, L. Balembois, J. Travesedo, M. Le Dantec, M. Rančić, E. Albertinale, R. Truong, S. Bertaina, T. Chanelière, P. Goldner, D. Estève, D. Vion, E. Flurin, and P. Bertet, Phys. Rev. Res. **7**, 013011 (2025).
[106]M. Le Dantec, M. Rančić, S. Lin, E. Billaud, V. Ranjan, D. Flanigan, S. Bertaina, T. Chanelière, P. Goldner, A. Erb, R. B. Liu, D. Estève, D. Vion, E. Flurin, and P. Bertet, Sci. Adv. **7**, eabj9786 (2021).
[107]Z. Wang, L. Balembois, M. Rančić, E. Billaud, M. Le Dantec, A. Ferrier, P. Goldner, S. Bertaina, T. Chanelière, D. Esteve, D. Vion, P. Bertet, and E. Flurin, Nature **619**, 276–281 (2023).
[108]J. Travesedo, J. O'Sullivan, L. Pallegoix, Z. W. Huang, P. Hogan, P. Goldner, T. Chaneliere, S. Bertaina, D. Estève, P. Abgrall, D. Vion, E. Flurin, and P. Bertet, Sci. Adv. **11**, eadu0581 (2025).

31 October 2026 16:32:36

© Author(s) 2026

[109]P. Neumann, J. Beck, M. Steiner, F. Rempp, H. Fedder, P. R. Hemmer, J. Wrachtrup, and F. Jelezko, Science **329**, 542–544 (2010).
[110]R. Vincent, S. Klyatskaya, M. Ruben, W. Wernsdorfer, and F. Balestro, Nature **488**, 357–360 (2012).
[111]J. J. Pla, K. Y. Tan, J. P. Dehollain, W. H. Lim, J. J. L. Morton, D. N. Jamieson, A. S. Dzurak, and A. Morello, Nature **489**, 541 (2012).
[112]M. H. Abobeih, Y. Wang, J. Randall, S. J. H. Loenen, C. E. Bradley, M. Markham, D. J. Twitchen, B. M. Terhal, and T. H. Taminiau, Nature **606**, 884–889 (2022).
[113]J. O'Sullivan, K. Reuer, A. Grigorev, X. Dai, A. Hernández-Antón, M. H. Muñoz-Arias, C. Hellings, A. Flasby, D. Colao Zanuz, J.-C. Besse, A. Blais, D. Malz, C. Eichler, and A. Wallraff, Nat. Commun. **16**, 5505 (2025).
[114]M. Stern, "Introduction to superconducting quantum circuits," in *New Trends and Platforms for Quantum Technologies* (Springer Nature, Switzerland, 2024), pp. 61–132.
[115]J. E. Mooij, T. P. Orlando, L. Levitov, L. Tian, C. H. van der Wal, and S. Lloyd, Science **285**, 1036 (1999).
[116]F. Yoshihara, K. Harrabi, A. O. Niskanen, Y. Nakamura, and J. S. Tsai, Phys. Rev. Lett. **97**, 167001 (2006).
[117]J. Bylander, S. Gustavsson, F. Yan, F. Yoshihara, K. Harrabi, G. Fitch, D. G. Cory, Y. Nakamura, J.-S. Tsai, and W. D. Oliver, Nat. Phys. **7**, 565 (2011).
[118]M. Stern, G. Catelani, Y. Kubo, C. Grezes, A. Bienfait, D. Vion, D. Esteve, and P. Bertet, Phys. Rev. Lett. **113**, 123601 (2014).
[119]T. P. Orlando, J. E. Mooij, L. Tian, C. H. van der Wal, L. S. Levitov, S. Lloyd, and J. J. Mazo, Phys. Rev. B **60**, 15398 (1999).
[120]D. Marcos, M. Wubs, J. M. Taylor, R. Aguado, M. D. Lukin, and A. S. Sørensen, Phys. Rev. Lett. **105**, 210501 (2010).
[121]J. Twamley and S. D. Barrett, Phys. Rev. B **81**, 241202 (2010).
[122]T. Douce, M. Stern, N. Zagury, P. Bertet, and P. Milman, Phys. Rev. A **92**, 052335 (2015).
[123]P. Bertet, I. Chiorescu, G. Burkard, K. Semba, C. J. P. M. Harmans, D. P. DiVincenzo, and J. E. Mooij, Phys. Rev. Lett. **95**, 257002 (2005).
[124]F. Yan, S. Gustavsson, A. Kamal, J. Birenbaum, A. P. Sears, D. Hover, T. J. Gudmundsen, D. Rosenberg, G. Samach, S. Weber, J. L. Yoder, T. P. Orlando, J. Clarke, A. J. Kerman, and W. D. Oliver, Nat. Commun. **7**, 12964 (2016).
[125]T. Chang, I. Holzman, T. Cohen, B. C. Johnson, D. N. Jamieson, and M. Stern, Phys. Rev. Appl. **18**, 064062 (2022).
[126]T. Chang, I. Holzman, S. Q. Lim, D. Holmes, B. C. Johnson, D. N. Jamieson, and M. Stern, Nat. Commun. **16**, 9832 (2025).
[127]R. E. George, W. Witzel, H. Riemann, N. V. Abrosimov, N. Nötzel, M. L. W. Thewalt, and J. J. L. Morton, Phys. Rev. Lett. **105**, 067601 (2010).
[128]D. Holmes, W. I. L. Lawrie, B. C. Johnson, A. Asadpoordarvish, J. C. McCallum, D. R. McCamey, and D. N. Jamieson, Phys. Rev. Mater. **3**, 083403 (2019).
[129]G. Wolfowicz, A. M. Tyryshkin, R. E. George, H. Riemann, N. V. Abrosimov, P. Becker, H.-J. Pohl, M. L. W. Thewalt, S. A. Lyon, and J. J. L. Morton, Nat. Nanotechnol. **8**, 561–564 (2013).
[130]V. Ranjan, B. Albanese, E. Albertinale, E. Billaud, D. Flanigan, J. J. Pla, T. Schenkel, D. Vion, D. Esteve, E. Flurin, J. J. L. Morton, Y. M. Niquet, and P. Bertet, Phys. Rev. X **11**, 031036 (2021).
[131]G. Ithier, E. Collin, P. Joyez, P. J. Meeson, D. Vion, D. Esteve, F. Chiarello, A. Shnirman, Y. Makhlin, J. Schriefl, and G. Schön, Phys. Rev. B **72**, 134519 (2005).
[132]M. Šimėnas, J. O'Sullivan, O. W. Kennedy, S. Lin, S. Fearn, C. W. Zollitsch, G. Dold, T. Schmitt, P. Schüffelgen, R.-B. Liu, and J. J. L. Morton, Phys. Rev. Lett. **129**, 117701 (2022).
[133]X. Yu, B. Wilhelm, D. Holmes, A. Vaartjes, D. Schwienbacher, M. Nurizzo, A. Kringhøj, M. R. v Blankenstein, A. M. Jakob, P. Gupta, F. E. Hudson, K. M. Itoh, R. J. Murray, R. Blume-Kohout, T. D. Ladd, N. Anand, A. S. Dzurak, B. C. Sanders, D. N. Jamieson, and A. Morello, Nat. Phys. **21**, 362–367 (2025).

31 October 2026 16:32:36

© Author(s) 2026